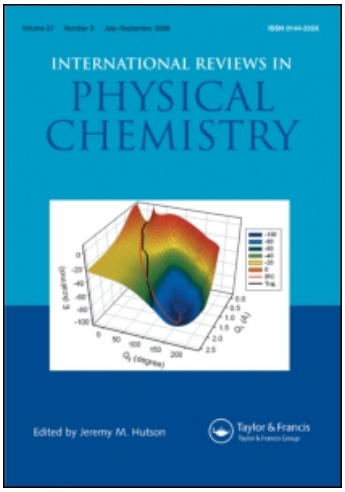

International Reviews in Physical Chemistry
Publication details, including instructions for authors and subscription information:
http://www.informaworld.com/smpp/title~content=t713724383

Interplay between theory and experiment in investigations of molecules embedded in superfluid helium nanodroplets

Krzysztof Szalewicz[a]
[a] Department of Physics and Astronomy, University of Delaware, Newark, DE 19716, USA

To cite this Article Szalewicz, Krzysztof(2008) 'Interplay between theory and experiment in investigations of molecules embedded in superfluid helium nanodroplets', International Reviews in Physical Chemistry, 27: 2, 273 — 316
To link to this Article: DOI: 10.1080/01442350801933485
URL: http://dx.doi.org/10.1080/01442350801933485

International Reviews in Physical Chemistry
Vol. 27, No. 2, April–June 2008, 273–316

Taylor & Francis
Taylor & Francis Group

Interplay between theory and experiment in investigations of molecules embedded in superfluid helium nanodroplets†

Krzysztof Szalewicz*

Department of Physics and Astronomy, University of Delaware, Newark, DE 19716, USA

(*Received 25 October 2007; final version received 20 January 2008*)

Helium is the only substance that has been observed on macroscopic scale to form the fourth state of matter, the superfluid state. However, until recently superfluid helium had not found any practical applications, mainly because it expels all other atoms or molecules. Only in the 1990s was it discovered that it is possible to mix in other substances with superfluid helium if helium is prepared as small droplets, called nanodroplets, containing only a few thousand atoms. This discovery led to the development of a new and very powerful experimental technique, called helium-nanodroplet spectroscopy. Superfluid helium creates a gentle matrix around the impurities and – due to superfluidity and to very weak interactions of helium atoms with other atoms or molecules – allows measurements of the spectra with precision not much lower than in the gas phase. Consequently, helium-nanodroplet spectroscopy enables very accurate probing of molecules or clusters which cannot be investigated in the gas phase due to their instability. This category includes 'fragile' molecules, isomers, radicals, and clusters in secondary minima. The major experimental developments will be described, emphasizing their importance for understanding basic principles of physics and new insights into chemically relevant processes.

The experiments have been assisted by theoretical work on impurity–He_n clusters. Most such work involves first-principles quantum simulations. Although the number of helium atoms that can be included in such simulations is significantly smaller than in a typical nanodroplet, theory explains most of the observed trends reasonably well. Theoretical results can also be compared directly and much more precisely than in the case of the droplets with the results of molecular beam experiments on clusters of controllable size, with the number of helium atoms ranging from 1 to almost 100. Most of the simulations published to date will be discussed and the level of agreement with experiment will be critically evaluated. The results of the simulations are very sensitive to details of the He–He and impurity–He interaction potentials used, and most of the current discrepancies between theory and experiment can be traced down to the uncertainties of the potentials. Thus, an important component of this review will be an analysis of various sources of errors in potential energy surfaces.

Keywords: Superfluid helium; helium nanodroplets; superfluidity; Bose–Einstein condensation; matrix isolation spectroscopy; molecular clusters

*Corresponding author. Email: szalewic@udel.edu
†Dedicated to Roger E. Miller.

ISSN 0144–235X print/ISSN 1366–591X online

DOI: 10.1080/01442350801933485
http://www.informaworld.com

Contents PAGE

1. Introduction

Superfluidity is the tendency of liquid helium to flow freely, even upward, with little apparent friction. This phenomenon can be observed if the temperature of helium is lower than 2.19 K (the so-called λ-point temperature). Superfluidity was discovered by Kapitza [1], and Allen and Misener [2] in 1937. It takes place only for the ^{4}He isotope of helium, which is a boson (at much lower temperatures, also the fermionic ^{3}He isotope becomes superfluid after bosonic pairs of such atoms are formed). In the independent-particle approximation, i.e. when the wavefunction for a set of identical particles (here atoms) can be written as a symmetrized or antisymmetrized product of single-particle wavefunctions, any number of bosons can occupy a given single-particle energy level (in contrast, only one fermion may occupy a given level). In consequence,

at very low temperatures, bosonic atoms occupy only the lowest energy levels. If one of these levels is macroscopically occupied, i.e. the majority of atoms are in the same single-particle state, these atoms carry no entropy. Furthermore, one can easily show that the flow of these particles is irrotational (see, for example, Ref. [3]). In 1941, Landau [4] intuitively postulated these two conditions and concluded from them that the excitation energy ϵ of the superfluid phase is a function of the momentum p transferred in the excitation. This is similar to collective excitations of solids, i.e. to phonons. In fact, Landau assumed that for superfluid helium the dependence $\epsilon(p)$ is linear for small p, i.e. the same as for phonons, but for larger p it goes through a maximum (called a maxon) and then a minimum (called a roton). These phenomenological assumptions were backed up in 1956 by theoretical arguments in the work of Feynman and Cohen [5]. With the assumed shape of $\epsilon(p)$, elementary arguments of momentum and energy conservation show [6] that a body moving through superfluid helium will encounter no drag forces below some critical velocity due to the fact that small-energy excitations are not possible. The same reasons lead to flow without friction. The phenomenon of superfluidity is one of the very few macroscopic manifestations of the quantum character of matter and it has fascinated physicists since its discovery. Several Nobel Prizes were awarded for investigations of superfluidity [Landau (1962); Kapitza (1978); Lee–Osherhoff–Richardson (1996); Abrikosov–Ginzburg–Leggett (2003)]. Helium is the only superfluid substance observed so far in macroscopic amounts, although there are indications [7] that small ensembles of molecular hydrogen may also exhibit superfluidity and it is generally accepted that parts of neutron stars are superfluid [8].

Einstein predicted in 1924 [9,10] (extending the earlier work of Bose for photons [11]) that, at a sufficiently low temperature, non-interacting bosonic atoms should undergo a phase transition, now called the Bose–Einstein condensation (BEC). In the BEC state, a macroscopic fraction of bosons occupies the single-particle ground energy level. London suggested in 1938 [12] that superfluidity is connected to BEC. However, Landau always opposed this idea and considered BEC to be a pathology of a non-interacting gas of bosons. The theory of superfluidity, for which Landau received the Nobel Prize, does not involve BEC. On the other hand, known theoretical justifications of the two assumptions made by Landau require a macroscopic occupation of a single-particle state, like in BEC. The current opinion of many researchers investigating superfluid helium is well described by Leggett in a recent review [3]: 'However, there is one feature of this whole scenario that might leave one with a feeling of slight disquiet: in the sixty years since London's original proposal, while there has been almost universal belief that the key to superfluidity is indeed the onset of BEC at the λ-temperature, it has proved very difficult, if not impossible, to verify the existence of the latter phenomenon directly. The main evidence for it comes from high-energy neutron scattering and, very recently, from the spectrum of atoms evaporated from the surface of the liquid, and while both are certainly consistent with the existence of a condensate fraction of approximately 10%, neither can be said to establish it beyond all possible doubt'. For more discussion of these issues, see Ref. [13]. An undisputable Bose–Einstein condensate was achieved experimentally by Cornell, Wieman, Ketterle, Hulet, and their collaborators in 1995 [14–16] in microscopic samples of alkali atoms cooled to nanokelvin temperatures. Such samples also show some features characteristic of superfluidity [17].

One reason that the fundamental question about the relation between superfluidity and BEC could not be settled is that whereas macroscopic superfluid phenomena have been extensively studied experimentally, not much information is available at the microscopic level. This sparse knowledge is due to lack of appropriate probes: liquid helium naturally cleanses itself of impurities. Only in 1992 have Goyal *et al*. [18] shown that one can combine other substances with superfluid helium if helium is formed as small droplets, called nanodroplets, containing only a few thousand atoms. Actually, at that time, it was not clear whether such droplets are superfluid. This was shown by Hartmann *et al*. [19] in 1995 by precise measurements of spectra of molecular impurities in nanodroplets. These discoveries have greatly improved our understanding of the mechanisms of superfluidity, as helium-nanodroplet spectroscopy provided the first unique and precise probe of the superfluid helium medium on the atomic scale.

The ability of helium to form droplets has been known for almost a century. Such droplets were first observed by Kamerlingh-Onnes [20] in 1908 in the form of a 'helium fog'. A reemergence of investigations of helium droplets took place in the 1960s through 1980s in cluster beams (see Ref. [21] for a review). However, lack of suitable experimental probes led to diminishing interest in the subject. In 1990, Scheidemann *et al*. [22] showed by using mass spectroscopy that helium droplets can pick neon atoms. Goyal *et al*. [18] were able to attach or embed molecules in a droplet by passing a collimated beam of helium droplets (formed by free-jet expansion of pressurized helium gas from a low-temperature nozzle) via a pick-up chamber containing a molecular vapour. The doped droplets were then probed spectroscopically. When the impurity, such as an SF_6 molecule, absorbs a photon, a part of the droplet is evaporated when the excitation energy is relaxed to helium, which provides the signal. The signal was initially measured using bolometric techniques; later also mass-spectroscopy methods have been applied.

Helium droplets normally contain several thousand atoms or even millions of atoms, i.e. have a diameter of a few nanometres and therefore are often called nanodroplets. The smallest droplets that can be formed contain a few hundred atoms. This size is still much larger than sizes that are possible in quantum mechanical computer modelling of superfluid phenomena where one can include at the most a hundred or so helium atoms. Nevertheless, results of theoretical calculations have been found to compare well with experimental findings despite the size difference and therefore can be used to interpret measurements. Quantum mechanical calculations can determine the superfluid fraction of the liquid and whether some of the helium atoms form a condensate. These calculations can also predict the results of high-precision spectroscopic measurements of impurities contained in nanodroplets. Thus, comparisons of such measurements with the results of numerical simulations lead to a better microscopic understanding of superfluidity and its relation to BEC. This becomes the key strategy for investigations of the phenomena of superfluidity, probing it down to the scale of individual atoms. Theoretical calculations can also be compared with experiments on impurity–He_n clusters formed in molecular beams. The helium nanodroplet developments inspired a large number of beam experiments, with the controlled number of the helium atoms reaching about 80 [23–25], only an order of magnitude less than in the smallest nanodroplets. These experiments are very important since comparisons can be made with theoretical calculations on clusters of exactly the same size.

As already mentioned, the first proof that helium nanodroplets are actually superfluid was provided by Hartmann *et al.* [19] in 1995. These authors observed sharp, rotationally resolved spectra of an impurity in nanodroplets, whereas normal solvents significantly broaden spectral lines of impurities due to intermolecular interactions. Even taking into account that for the helium solvent such interactions are much smaller than for any other solvent, one expected broader lines than observed. The final proof was achieved in 1998 when the same group found only very broad spectral peaks in helium nanodroplets formed by the fermionic ^{3}He isotope [26]. They then added a small number of ^{4}He atoms to such droplets and showed that it requires only about 60 atoms to achieve the onset of superfluidity. This agrees with earlier theoretical predictions by Sindzingre *et al.* [27]. These experiments also determined the temperature of the droplets to be 0.38 K for ^{4}He and 0.15 K for ^{3}He. A similar method was used later by Grebenev *et al.* [7] to create a thin layer of parahydrogen molecules around a chromophore in a helium nanodroplet. Changes of the spectral patterns at a temperature of about 0.15 K indicate that this layer becomes superfluid at such temperature. This was the first observation of any substance other than helium to become superfluid (although, as mentioned above, microscopic ensembles of alkali atoms show some features of superfluidity).

Despite the fact that superfluidity in helium nanodroplets is identified by somewhat different characteristic features than in bulk liquid helium, it is rather clear that the same phenomenon is observed in both cases. In theoretical work on pure helium, the superfluidity can be determined by placing a helium cluster in a slowly rotating external field [27] to find the fractions of the classical and quantum response of the system, the latter being identified with superfluidity. The approach is analogous to the macroscopic Andronikashvili 'rotating bucket' experiment [28]. More recent theoretical papers use the concept of superfluidity even for impurity–He_n clusters containing only a few helium atoms. For example, Paesani *et al.* [29] find the onset of superfluidity already in CO_2–He_5. The fraction of atoms that are superfluid is defined by these authors as the ratio of the difference between the classical and quantum moments of inertia of the system to the former moment.

Equally important to probing the mechanisms of superfluidity, is the ability of the new technique to study molecules in novel ways. Clearly, the measurements of spectra of molecules embedded in superfluid helium nanodroplets not only give information about the properties of helium, but also about the impurity molecules. For molecules which can also be measured in the gas phase, the latter information does not provide new insights. However, there are many molecules which are too unstable to be studied in the gas phase. The techniques of embedding these types of molecules in various solvents to measure the spectra have been popular for a long time and are known under the name of matrix-isolation spectroscopy. The major drawback of these techniques is that even rare-gas matrices broaden the spectral lines rather significantly due to the van der Waals interactions between the matrix and the chromophore and, in the case of solid matrices, due to chromophores occupying different types of sites. The use of helium would minimize such interactions; however, macroscopic helium matrices cannot be used since helium expels impurities which then aggregate on the walls of the container. The use of helium nanodroplets has resolved this difficulty. In a recent experiment, Lehnig *et al.* measured a spectral line of NH_3 only 0.0005 cm^{-1} wide [30]. The helium-nanodroplet 'isolation' spectroscopy technique allows accurate measurements of spectra of many

molecules or clusters that cannot be obtained by any other methods. This includes 'fragile' molecules, molecular isomers, radicals, and clusters in secondary minima. Since the spectra are much sharper than those that can be obtained in any standard matrix-isolation measurements, a much better characterization of these molecules can be achieved. Therefore, for investigations of such molecules, helium-nanodroplet spectroscopy becomes the method of choice.

Helium-nanodroplet spectroscopy offers advantages also when applied to non-fragile molecules. The ability to cool molecules down to subkelvin temperatures greatly increases the range of properties that can be investigated. Thus, the method can also be viewed as providing a small refrigerator (a helium nanodroplet) for an individual molecule. The low-temperature environment is important, for example, in investigations of biomolecules. Although spectra of biomolecules can be measured using traditional techniques, such spectra are usually not possible to resolve, even for small biomolecules, due to the presence of many isomers with small isomerization barriers. In nanodroplets, the isomers become frozen and can be distinguished by applying an electric field. Thus, one can measure high-accuracy spectra that can be interpreted. This approach also allows studies of the isomerization phenomenon.

The range of spectroscopic techniques used to investigate molecules embedded in helium nanodroplets steadily increases, which in turn increases the range of phenomena that can be investigated. Whereas the methods of infrared (rovibrational) and microwave (rotational) spectroscopy have been used most often, electronic spectroscopy has also been routinely applied. Recently, photoelectron spectra of molecules embedded in helium nanodroplets have been measured [31]. Many of the newer experiments are of pump-probe type, which is particularly important for investigations of the dynamics of chemical reactions. Since chemical processes become very slow at nanodroplet temperatures, different stages of a reaction can be observed. Helium nanodroplet spectroscopy also allows characterization of prereactive complexes, which have been shown to be of critical importance for predicting the outcome the chemical reactions. The nanodroplets can even be used to synthesize compounds that cannot be made in other environments. While this cannot be a practical method for producing new materials, it allows their characterization which may lead to alternative ways of synthesis if such materials turn out to be of significant interest. Another possible application of helium nanodroplets could be for assembly, transport, and surface deposition of atomic or molecular clusters [32].

The developments of helium-nanodroplet spectroscopy have been reviewed by several authors [33–41]. These reviews concentrated mostly on the experimental aspects of the phenomena, except for Refs. [40] and [41]. The present paper will emphasize theoretical developments, but from the point of view of the interplay between theory and experiment. As we will see, this interplay resulted in significant progress in the field. The microscopic picture based on *ab initio* predictions critically depends on the use of realistic intermolecular interaction potentials. There is a clear connection between the strengths and topologies of intermolecular potential energy surfaces and the properties of molecules embedded in helium nanodroplets and in helium clusters. Ultimately, these are the potential surfaces that determine the results of experiments. A better understanding of these relations will not only increase our ability to interpret experiments, but will enable creation of clusters with tailor-made properties.

2. Experimental spectra of impurities in helium nanodroplets

Since the first measurement of spectra of a molecule within a helium nanodroplet [18], a large number of molecules, ions, radicals, and clusters have been investigated experimentally; see, for example, Refs. [19,33–39,42–55]. This list is by no means complete and several other experiments will be discussed later on. As already stated, there are two main reasons for such a broad interest in this experimental technique: (i) the very cold helium matrix allows preparation of structures which are not possible to assemble in any other way; (ii) the spectra in the droplets resemble the corresponding gas-phase spectra. The latter is a highly non-trivial property and it is directly related to the superfluidity of the nanodroplets.

The precision of gas-phase spectroscopical measurements is among the highest of all types of measurements and this method often achieves $0.0001\,cm^{-1}$ resolution. Some species whose spectra cannot be measured in gas phase have been investigated for a long time in low-temperature matrices, most often in argon or neon matrices. However, the resolution then decreases to only about $1\,cm^{-1}$. This is due to intermolecular interactions between the molecule embedded in the matrix and the atoms of the matrix. The typical spectra of molecules in solutions are even less resolved and consist of broad peaks without any characteristic spectral patterns. The use of helium as the matrix was always recognized as an important goal since helium interacts with molecules even weaker than neon or argon. For example, the depths of the He–HCN, Ne–HCN, and Ar–HCN interaction potentials are $30\,cm^{-1}$ [56], $63\,cm^{-1}$ [57], and $147\,cm^{-1}$ [56], respectively. Thus, a helium matrix should provide a better resolution than the neon or argon one, although still of the order of $1\,cm^{-1}$. However, due to superfluidity, the lines of the spectra measured in helium nanodroplets are in fact much sharper and can be resolved to $0.01\,cm^{-1}$ or better (even, in exceptional cases, to $0.0005\,cm^{-1}$ [30]). There are some spectral regions, however, with a significant broadening of lines in the case of levels that can relax with energy transfer of about $10\,cm^{-1}$ which couples to roton excitations in helium. One should also mention here that one additional advantage of helium-nanodroplet spectroscopy is that helium remains optically transparent up to about $160{,}000\,cm^{-1}$. In the case of spectra taken in solutions, lines of the solvent often obscure the lines of the solute.

Whereas the first spectrum of a molecule in helium nanodroplets had a relatively low resolution [18], a few years later Hartmann *et al.* [19] performed an experiment that was precise enough to resolve the rotational lines in the vibrational spectrum of SF_6. An analysis of rotational transitions allowed the authors to determine the temperature of the droplet to be 0.37 K (later this number was slightly revised and one currently assumes that the temperature is 0.38 K). Since the spectra were resolved to better than $0.1\,cm^{-1}$, it was immediately clear that this must be due not only to the diminished intermolecular interactions of SF_6 with helium compared to neon or argon, but also due to superfluidity of helium. That this is indeed the case was demonstrated beyond doubt by a very elegant experiment by Grebenev *et al.* in 1998 [26] (see also Refs. [42,43]). These authors formed droplets using the fermionic ^3He isotope which does not become superfluid until the temperature reaches 0.003 K. Indeed, the spectra of OCS in ^3He nanodroplets were completely unresolved, exhibiting about $1\,cm^{-1}$ broad peaks, whereas in ^4He nanodroplets the width of the peaks was of the order of $0.01\,cm^{-1}$ and these peaks could be identified as specific rovibrational excitations of OCS. The same

work investigated also the very important question of how many ^{4}He atoms are needed for a helium cluster to become superfluid. The authors were able to do so by doping the ^{3}He droplets containing embedded OCS molecules with ^{4}He atoms. The latter isotope tends to concentrate around the impurity due to slightly stronger binding resulting from lower zero-point energy. The experimental finding was that the onset of superfluidity takes place with about 60 ^{4}He atoms in the droplet. This very important finding confirms earlier theoretical predictions [27] based on path integral Monte Carlo calculations. The work of Grebenev *et al.* [26] also found that the temperature of the ^{3}He nanodroplets is 0.15 K. One should mention here that some earlier experimental evidence of superfluidity of the droplets came from the work of Hartmann *et al.* [58] who measured the spectrum of electronic excitations of glyoxal in ^{4}He nanodroplets. The authors found in this spectrum the phonon wing with features related to the maxon and roton and a distinct gap between this wing and the zero phonon line. Such features are characteristic of superfluidity. In 2000, Grebenev *et al.* [59] repeated the same experiment in ^{3}He nanodroplets. No gap or maxon/roton features were observed.

Nanodroplet spectroscopy has also provided some evidence that hydrogen may become superfluid at low temperatures. Grebenev *et al.* [7] measured the spectra of OCS in nanodroplets containing a number of parahydrogen molecules. Due to the fact that H_2 interacts stronger with OCS than He, one expects that OCS will be surrounded by a layer of parahydrogen within the helium nanodroplet and helium serves in this case only as a cryostat. When all the helium was in the form of ^{4}He, the spectra showed characteristic rovibrational lines identified as rotational Q branches resulting from the motion of $(H_2)_n$–OCS complexes around the OCS axis. These branches disappeared when ^{3}He was added. Since this addition lowered the temperature of the droplet from 0.38 K to 0.15 K, the authors interpreted the observation as evidence that parahydrogen became superfluid due to this temperature drop and stopped rotating around OCS. This interpretation was later supported by theoretical studies [60].

It should be clear from this discussion that the properties of helium nanodroplets have been well understood by now. The nanodroplets therefore provide a well characterized, very low-temperature medium for high-accuracy spectroscopic investigations of atoms, molecules, radicals, clusters, and nanocrystals. This technique also opens up the possibilities for growing new types of molecules, clusters, and nanomaterials. Several such applications will be described below.

The initial applications of helium-nanodroplet spectroscopy embedded in the droplets just single molecules such as sulfur hexafluoride, SF_6 [18,19], carbonyl sulfide, OCS [26], or glyoxal, $H_2C_2O_2$ [58]. Such studies have continued since the experiments found several interesting similarities and differences in the behaviour of various molecules. Although, as discussed above, the rovibrational spectra of molecules in liquid nanodroplets resemble the spectra in the gas phase, for most molecules the rotational constants significantly decrease in the droplets, as seen for the first time by Hartmann *et al.* [19] in 1995. The decrease is small only for molecules that rotate very fast, i.e. have very large constants in the gas phase (see Table I in Ref. [34] and Table 3 in Ref. [37] for experimental values of both types of constants). One exception is the LiH molecule which rotates fast but undergoes a very significant reduction of the rotational constant [61]. The simplest explanation of the decrease of rotational constants, i.e. increase in the moment of inertia,

is 'sticking' of the helium atoms to the molecules; see Section 4 for a discussion of these issues.

The next group of systems that have been often investigated in helium nanodroplets are molecular clusters. The first such observation, involving the $(SF_6)_n$ and $Rg–SF_6$ clusters, where Rg = Ne, Ar, Kr, or Xe, was published in 1996 [62]. The formation of clusters in nanodroplets is very natural since, due to the small size of the droplets and the smallness of He–molecule interactions compared to molecule–molecule interactions, if several molecules are picked up by a droplet, these molecules will quickly find each other to form a cluster. Perhaps a surprising discovery in this field was that the molecules often form very unusual clusters, such as the linear $(HCN)_n$ structures with n up to 7 [63] or the cyclic water hexamer [46]. In the gas phase, such clusters represent local minima on the potential energy surfaces and cannot be observed since the systems end up in global minima. The superfluid helium matrix stabilizes local minima structures and allows their spectral detection. The cluster growth can be controlled to some extent in experiments, resulting in the possibilities of designing and producing new types of clusters. The main type of control is a sequential pick-up process. A good example is $Ar_n–HF$ clusters investigated by Nauta and Miller [64]. If argon atoms are inserted into a droplet first and a HF molecule is added next, a small quasi-sphere of argon is formed with HF attached to the surface of the sphere. If the order is reversed, HF becomes coated with argon atoms [64]. Another mechanism providing some control is the utilization of long-range electrostatic forces. Dimers of linear molecules that form hydrogen bonds can be either linear, like $(HCN)_2$ [65], or nonlinear, like $(HF)_2$ [66]. However, the trimers of such molecules, even of those that form linear dimers, will always be cyclic simply because the formation of one more intermolecular bond in the cyclic geometry energetically outweighs the increase of the energy due to the bending of dimer bonds. Linear trimers and larger linear clusters of molecules that form linear dimers usually constitute local minima on potential energy surfaces. In helium nanodroplets, it has been possible to form complexes in such local minima by utilizing the long-range behaviour of intermolecular potentials. A very nice example of such work is the investigation of $(HCN)_n$ clusters by Nauta and Miller [63]. First, an HCN dimer is formed in a droplet and it is, predictably, linear, as in the gas phase. When a third monomer is added, at large intermolecular separations it will align itself with the dimer. This is because, at such separations, the dipolar interactions dominate the potential due to their slowest, $1/R^3$, decay and the minimum of the dipole–dipole interaction potential is at the linear configuration. As the monomer approaches the dimer, it does not get out of the local minimum since the kinetic energy of relative motion is constantly dissipated to the helium environment. One sometimes says that the solvent assures a 'soft landing' of molecules when a complex is formed. Nauta and Miller utilized this property to form linear chains containing up to seven HCN molecules [63]. Local minima clusters are an interesting but only a special case of investigations of clusters in helium nanodroplets. Many other clusters were found in configurations similar to gas phase configurations. Still, interesting information can be obtained from measurements in the droplets, for example, about tunnelling splittings in hydrogen-bonded complexes.

Helium nanodroplets can stabilize not only unusual clusters but also free radicals, systems of utmost importance for understanding chemical reactions. Radical can be produced by pyrolysis or photolysis of molecules, but their concentrations in the gas

phase are insufficient for performing measurements. The classical matrix isolation techniques have been widely used to stabilize radicals. As discussed earlier, a limitation of these techniques is that the spectral resolution is of the order of $1\,cm^{-1}$. Helium nanodroplet spectroscopy allows similar studies with a resolution at least an order of magnitude better. Even more important than investigations of isolated free radicals are measurements of complexes of radicals with other molecules, which allow direct probings of processes in the entrance or exit channels of chemical reactions. All these subjects have recently been reviewed by Küpper and Merritt [67]. Helium nanodroplet spectroscopy even allows some studies of the dynamics of chemical processes; see for example the investigations of photoinduced dynamics of high-spin alkali trimers [68], manipulations of the $Ba + N_2O \rightarrow BaO + N_2$ reaction [69], or studies of the photodissociation of CH_3I [70]. Due to the very low temperature of the droplets, chemical processes are significantly slowed down, which may perhaps allow time-resolved future studies and chemical synthesis of novel compounds.

A special class of systems investigated by helium-nanodroplet spectroscopy are biomolecules and clusters of biomolecules with water. The molecules investigated, such as tryptophan, $C_{11}H_{12}N_2O_2$ [71,72], are very small among biomolecules, but are at the same time very complicated systems from the point of view of the interpretation of the rovibrational spectra. Such assignments are possible in nanodroplets due to the possibility of controlling molecular orientations by electric fields. The rapid cooling of biomolecules by the droplet results in freezing of tautomers present at the initial temperature and therefore provides more information than one could anticipate. For example, in a recent study Choi and Miller [73] observed four tautomers of guanine. Helium-nanodroplet spectroscopy has also been applied to large molecules not related to biological processes, like for example to oligomers of 3,4,9,10-perylene-tetracarboxylic dianhydride (PTCDA) [74], a molecule with semiconducting properties that is of importance in electronic and optoelectronic applications. This work produced the first resolved electronic spectrum for such a system. One more type of very large molecules studied in this way are polycyclic aromatic hydrocarbons, including molecules as large as biphenylene [75] or benzo(k)fluoranthene, $C_{20}H_{12}$ [76].

One type of system often investigated by helium-nanodroplet spectroscopy is metal atoms and clusters [36,68,77–88], mostly applying electron-excitation spectroscopy. Due to the large energies of such excitations, a larger degree of solvent perturbation is involved. This feature makes the investigations of the clusters more difficult, but at the same time allows better probing of the environment, including time-resolved studies. One important question to be answered is whether such clusters reside on the surface or inside a droplet [36,68,77–88]. This behaviour depends on the strength of the He–metal interaction. The depths of such interaction potentials, D_e, are very small and cannot be measured. Thus, the only information about this quantity comes from *ab initio* calculations; see the further discussion in Section 4. The alkaline atoms always reside on the surface of the droplet [80,89,90], whereas alkaline earth atoms are a borderline case and their location depends on the atomic number and may depend on the isotope of helium [83,91]. Therefore, heavier alkaline earth atoms may provide an important probe of mixed ^{3}He–^{4}He droplets [91]. One may note that all known molecule–He interactions are significantly stronger than He–He interactions. Thus, all molecules end up inside the droplets.

Although there are important issues concerning physics of single atoms, see for example the time-resolved measurements of excitations of Al [92], the main theme of investigations of metals embedded in or attached to the surface of the nanodroplets are studies of small metal clusters. The ultimate goal of such studies is a better understanding of the structure and properties of metals. For example, sodium dimer and trimer were studied in Refs. [77,78,93]. This work provided precise data for the dimer in the triplet state and the first characterization of the trimer in the quartet state. The latter system was found to exhibit extremely strong non-additive interactions [94,95].

3. Pure helium

In order to model a molecule–He_n cluster with $n > 1$ or to model superfluid pure helium, one has to know the interaction potential between helium atoms. Knowledge of this potential is also important for many other applications of helium in science and industry. In particular, helium is used as a benchmark system in thermal physics [96,97] since it is closest to an ideal gas. The deviations of helium gas from ideality can be measured or computed from first principles. In recent years, the latter approach was able to provide more accurate values for these deviations than the former one. Since this accuracy determines our ability to establish better international thermodynamic standards (e.g. of temperature and pressure) [96], *ab initio* calculations of the interaction potential for the helium dimer have been pursued by a large number of research groups in recent years [98–112]. The current state of thermodynamics standards and their relation to the thermophysics of helium is discussed in Ref. [113].

Intermolecular interaction energies can be computed using the supermolecular (SM) approach, i.e. subtracting the total energies of monomers from the total energy of a dimer, or using symmetry-adapted perturbation theory (SAPT) [113–115], i.e. calculating the interaction energies directly as perturbative corrections (relative to the energies of infinitely separated monomers). In the former approach, one can use in principle any standard electronic structure method and virtually all available methods have been applied to He_2. Due to the smallness of the helium dimer interaction energy, size-consistent methods have to be used, i.e. methods having the property that the dimer energy converges to the sum of monomer energies for very large interatomic separations R. With the current accuracy goals, the interaction energy is usually computed using several different methods at the same time. Lower level and therefore computationally more efficient methods are applied with larger basis sets and more expensive high-level calculations are performed in smaller bases. In recent years, the most popular method of the first type has been the coupled-cluster theory with single, double, and non-iterative triple excitations, CCSD(T) [116,117]. For larger systems, less expensive many-body perturbation theory at nth-order level, $n = 2$–4 (MBPTn) [118], is also often used. This method is sometimes called MPn if the Møller–Plesset partition of the Hamiltonian [119] is applied. At the highest level, one has now to use the full configuration interaction (FCI) method which is equivalent to the exact solution of the Schrödinger equation in a given orbital basis set. The SM interaction energies always have to be computed using the counterpoise (CP) method [102,120–124] to remove the basis set superposition error (BSSE). Although BSSE vanishes in the limit of the complete basis set and becomes very small in the largest

basis sets used in some recent calculations, it is always comparable to uncertainties resulting from basis set incompleteness.

The SAPT approach is usually applied at the second or third order in the intermolecular perturbation operator V [113,114,125]. However, for the interaction of two-electron systems, a special program has been developed which allows calculations to arbitrary order [102,123]. The convergence properties of SAPT have been extensively studied [126–130] – for a review see Ref. [113] – and for He_2 several versions of SAPT converge well. The limit value of the interaction energy agrees very well with the interaction energy computed in the same orbital basis set using the CP-corrected FCI method. This, in fact, provides one of the best arguments for the correctness of the CP method of removing BSSE since SAPT is by definition BSSE free.

SAPT calculations for He_2 date back to the 1970s [131,132] and continued in the 1980s [133–135]. The complete potential was produced in 1996 [101,102] and has since become the most often used *ab initio* potential for the helium dimer (it will be called SAPT96 below). It has, in particular, been applied to calibrate thermophysical measurements [96]. An important element of the SAPT calculations for He_2 has been the use of explicitly correlated basis sets in the form of the so-called Gaussian-type geminals (GTG), i.e. functions with an exponential dependence on the square of the interelectronic distance. This basis set is complete [136,137] and leads to significantly more accurate interaction energies than calculations using orbital bases which are slowly converging due to the difficulties in reproducing the electron–electron cusps. The GTG bases can also be applied in standard correlation energy calculations [138–144]. These bases were used to describe the bulk of the He_2 interaction energy, whereas a small remaining contribution was computed using orbital basis sets.

Recently, the calculations of Refs. [101,102] have been revisited [111,112]. Several methodological improvements have been developed and basis sets much larger than before were used. A major improvement was an application of extrapolations to the complete basis set (CBS) limit in the orbital calculations. Another one was the use of the SM approach for smaller R and of SAPT for larger R, depending on the error estimates. The performance of CBS extrapolations was tested against GTG results on terms that can be computed both ways [108,109]. In the SM calculations [111], the major part of the interaction energy was obtained using the GTG implementation of the coupled cluster theory at the double excitations level (CCD) [141] and for some distances at the single and double excitations level (CCSD) [145]. Relatively small contributions from triple and quadruple excitations were subsequently included employing the orbital CCSD(T) and the FCI methods and using very large basis sets – up to doubly augmented septuple- and sextuple-zeta size, respectively, supplemented by mid-bond functions. These calculations were followed by extrapolations to the CBS limits. In SAPT calculations [112], the first-order interaction energy and the bulk of the second-order contribution were obtained using GTG basis sets and were converged to about 0.1 millikelvin (mK) near the minimum and for larger R. The remaining second-order contributions available in the SAPT suite of codes were computed using very large orbital basis sets, up to septuple-zeta quality, augmented by diffuse and mid-bond functions. The accuracy reached at this level was better than 1 mK in the same region. Since, as discussed above, high-order SAPT calculations converge to FCI results for He_2, and the FCI approach is computationally more efficient, all the remaining

components of the interaction energy were computed using the FCI method in bases up to sextuple-zeta quality. The latter components, although contributing only 1% near the minimum, have the largest uncertainty of about 10 mK in this region. The SM results for $R \leq 6.5$ bohr were combined with the SAPT results from 7.0 to 12 bohr to fit analytic functions for the potential and for its error bars. The potential fit uses the best available van der Waals constants C_6 through C_{16}, including C_{11}, C_{13}, and C_{15}, and is believed to be the best current representation of the Born–Oppenheimer (BO) potential for helium. The fit exhibits the well depth $D_e = 11.006 \pm 0.004$ K and the equilibrium distance $R_e = 5.608 \pm 0.012$ bohr. Since the total energy of the dimer is about 6 atomic units, an accuracy of 2 ppb has been achieved. Compared to the 1996 SAPT potential, the uncertainties have been decreased by more than an order of magnitude. We will refer to the potential of Refs. [111,112] as CCSAPT07.

The estimates of uncertainties given above are not rigorous, but are believed to be reliable. Such estimates are obtained by analysing the rate of convergence of the results with basis set size and performing extrapolations to the CBS limits in several different ways. The reliability of past estimates can be evaluated as more accurate calculations become available. For example, the uncertainties of the SAPT96 potential [101,102] are for most points consistent with the CCSAPT07 potential. Only for a few points, including the minimum separation, were the uncertainties underestimated by up to about a factor of 2. The reliability of the estimates can also be tested by large-scale calculations using completely different methods. The comparisons of the CCSAPT07 potential with the results of quantum Monte Carlo calculations [110] and four-electron explicitly correlated calculations [146] fully support the error estimates of Refs. [111,112].

With the accuracy level achieved, various post-BO effects become comparable or even larger than the BO-level uncertainties. The most important post-BO contributions are the adiabatic (diagonal) correction [147], relativistic corrections [148], and quantum electrodynamics corrections [149]. At the van der Waals minimum distance, the largest of such corrections are of the order of 10 mK (but there is a mutual cancellation among them). These corrections have recently been computed for a large enough number of interatomic separations to fit a potential and the results for finite R have been smoothly connected with the asymptotic dependence [150].

The internal estimates of uncertainties can be supported by using the potential to compute various observables and comparing them to experimental data. The potential of Ref. [112] was applied to the calculation of the properties of the bound state of $^4He_2$. This very unusual, extremely extended molecule is difficult to study experimentally [151–153]. The asymptotic retardation correction was added to the BO potential at all separations. The computed value of $\langle R \rangle = 47.8$ Å (using atomic masses in nuclear dynamics calculations) is consistent with the best measurement of this quantity from Ref. [153], which gave $\langle R \rangle = 52 \pm 4$ Å. The dissociation energy of 1.56 mK is about 10% above the upper limit of the measured value amounting to $1.1 + 0.3/-0.2$ mK. The scattering length is equal to 91.8 Å. Thus, the agreement between theory and experiment on the bound state of the helium dimer provides additional support of the estimates of uncertainty made in Refs. [111,112].

The CCSAPT07 potential has not yet been applied in calculations of thermophysical properties of helium, but SAPT96 has been used extensively [96,154]. The latter potential predicted the properties better than any earlier helium dimer potential. Hurley

and Moldover [96] concluded: 'we recommend the *ab initio* results be used as standards for calibrating instruments relying on these thermophysical properties'. It is expected that the CCSAPT07 potential will result in even more accurate predictions and will allow the construction of new temperature and pressure standards based on *ab initio* calculations.

The CCSAPT07 potential is compared in Figure 1 with the SAPT96 potential and the most often used empirical potentials: HFDHE2 [155], HFD-B(HE) [156], and LM2M2 [157]. Plotted are the differences between a given potential and CCSAPT07. Also the error bars of CCSAPT07 are plotted (these error bars are too small to be visible in the first panel). Figure 1 shows that all the differences are significantly larger than the error bars of CCSAPT07. The two older empirical potentials, often used in simulations of helium, are significantly less accurate than the SAPT96 potential. Interestingly enough, the accuracy of the least popular of the three empirical potentials, LM2M2 [157], is comparable to that of SAPT96. One should point out, however, that LM2M2 is not a typical empirical potential but rather an *ab initio* potential tuned to improve agreement with experiment. Aziz and Slaman [157] first fitted several potentials to the interaction energies computed by Liu and McLean [158] and by van Duijneveldt *et al.* [159,160]. Then some parameters in these potentials were carefully changed to reduce discrepancies with experiment without significant departures of the potential from the computed points.

In order to model helium nanodroplets or bulk helium, one also needs to know pairwise non-additive interactions between helium atoms. Although such interactions are fairly small and have been neglected in most previous work, with the increased precision of pair potentials, the three-body non-additive contributions have to be taken into account. Surprisingly, no accurate non-additive potential has been available in the literature until recently, except for the potential of Ref. [161] which has, however, a very complicated form. The older three-body non-additive helium potentials [162–164] are simple but of rather low accuracy compared to more recent results (see the discussion of these potentials in Ref. [161]) and have been found to deteriorate the agreement with experiment [165] when used in simulations of condensed helium. An accurate and reasonably simple potential fit of helium three-body non-additive interaction energy has been published recently [166] using both the SM approach at the CCSD(T) level and the three-body SAPT method [161,167]. Large basis sets were applied, up to the quintuple-zeta doubly-augmented size. The fitting functions were similar to those developed in Refs. [168,169] and contained an exponentially decaying component describing the short-range interactions and damped inverse powers expansions for the third- and fourth-order dispersion contributions. The largest uncertainty of the potential comes from the truncation of the level of theory and can be estimated to be about 10 mK or 10% at the trimer's minimum configuration. The relative uncertainties for other configurations are also expected to be about 10% except for regions where the non-additive contribution crosses zero. Such uncertainties are of the same order of magnitude as the current uncertainties of the two-body part of the potential.

The new global non-additive potential [166] made possible precise comparisons of the three-body to two-body effects. Figure 2 of Ref. [166] plots such a ratio for a broad range of isosceles triangle geometries. For configurations with separations larger than the minimum separation, the three-body energies are smaller than 0.1% of the two-body term. However, in the region of the minimum, this ratio is larger and amounts to about

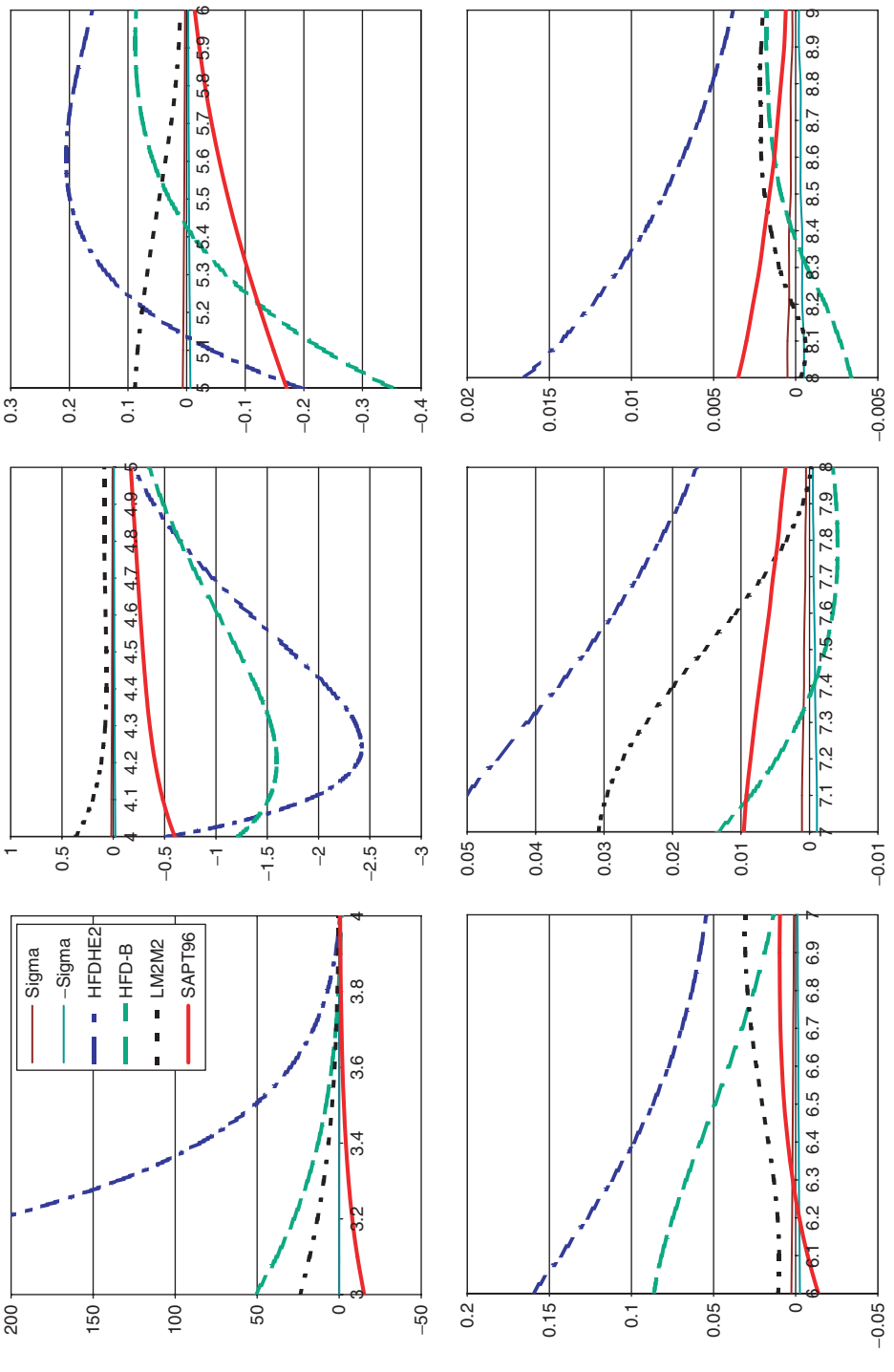

Figure 1. [Colour online] Comparison of He_2 potentials. Plotted are the differences between a given potential and the CCSAPT07 potential [112]. 'Sigma' are estimated error bars of the CCSAPT07 potential. The potentials HFDHE2, HFD-B, LM2M2, and SAPT96 are from Refs. [155], [156], [157], and [101,102], respectively. The distances are in bohrs and energies are in kelvins.

0.3%. When the interatomic distances are decreased further, at some point the two-body energy crosses zero, but the non-additive contribution remains approximately constant there. Thus, in this (relatively small) region, the three-body effects dominate the two-body ones. The ratio is also fairly large, of the order of 1%, for most strongly repulsive configurations.

Knowledge of the interactions between helium atoms allows one to perform simulations of pure helium. At low temperatures, helium exhibits a strong quantum character, therefore such calculations have to be performed applying quantum approaches. The most often used are path integral Monte Carlo (PIMC) [170] and density functional theory (DFT) [171] methods. The former is an *ab initio* method and gives results dependent on temperature. The latter is an empirical method, heavily parametrized on measured properties of liquid helium, and gives only $T = 0\,\mathrm{K}$ properties (although recently a T-dependent DFT approach has been developed [172]). At $T = 0$, also methods such as variational MC (VMC) or diffusion MC (DMC) [173] can be used. There are several versions of DMC, the two most often used for He_n–molecule clusters are the projection operator imaginary time spectral resolution (POITSE) method [174] and the reptation quantum Monte Carlo (RQMC) [175] method. The PIMC calculations for helium can be performed with periodic boundary conditions to represent bulk liquid or for helium clusters. At present, such calculations can be done with high numerical accuracy and represent liquid helium or nanodroplets very well. As mentioned in the Introduction, there is still considerable debate on how to identify superfluidity and BEC in microscopic calculations. In the case of superfluidity, one usually defines the superfluid behaviour by mimicking the macroscopic definition and placing the helium cluster in a slowly rotating external field [27] to find the fractions of the classical and quantum response of the system. Sindzingre *et al.* [27] have shown that already the $^4He_{64}$ cluster behaves similarly to bulk helium in that the normal fluid fraction decreases from one to zero between 2 K and 0 K. It is more difficult to determine the fraction of atoms that form BEC. The textbook descriptions of BEC hold only for non-interacting bosons and define BEC as macroscopic occupation of the ground-state wavefunction which is the symmetrized product of identical single-particle wavefunctions. However, for an interacting system, the ground-state wavefunction, even at $T = 0$, cannot be represented as such a product since excited symmetrized products are needed in the expansion to describe correlations between the particle motions. On the other hand, the ground-state single-particle function is also characterized by zero momentum of the particle. Thus, one may determine the probability that an atom is in such a state and use it as a measure of the condensate fraction. From Heisenberg's principle, the zero-momentum state corresponds to an infinite extent of the single-particle wavefunction in position space. The latter definition is more convenient to use in PIMC and the condensate fraction is determined as the large-distance limit of the single-particle density matrix. Calculations by Ceperley and Pollock [176] indicate that for $T \to 0\,\mathrm{K}$, the condensate fraction approaches 10%. More recent calculations give slightly smaller numbers. Moroni and Boninsegni [177] obtained $6.9 \pm 0.5\%$. This value agrees very well with neutron scattering measurements by Glyde *et al.* [178] which gave $7.25 \pm 0.75\%$. The most recent PIMC calculation by Boninsegni *et al.* [179] gave a value of about 8%. These calculations have smaller error bars than previous work and agree very well with the measured [178] condensate fractions for $T > 1.3\,\mathrm{K}$.

4. Atoms, molecules, and clusters in helium nanodroplets

Modelling of molecule–He_n clusters requires knowledge of the molecule–He potential. Several such potentials have been developed in the past decade. Often clusters of molecules are of interest; then in addition one has to know the interaction potentials between molecules and atoms constituting the cluster. We will start from the simplest case of a single molecule inside a cluster. As discussed earlier, the spectra of molecules in helium nanodroplets resemble gas-phase spectra except that the rotational constant B is decreased. For light rotors, the decrease is usually very small. For heavier rotors, the decrease is often close to a factor of three, although in some cases it is as large as six. In the first approximation, the trends can be explained by a very simple model assuming that a number of helium atoms stick to the impurity molecule and rotate with it [180]. It turned out that if the helium atoms are placed at the position that minimize the energy of a given molecules–He_n cluster and at the same time n is chosen such that the binding energy per helium atom is maximized, this simple model often gives near-quantitative results. One should emphasize, however, that this model does not capture any essential physics of the motion of an impurity molecule in superfluid helium. Much more reliable and physically sound predictions can be obtained from quantum MC calculations on molecule–He_n clusters, which show that a number of helium atoms adiabatically follow the motion of the molecule, resulting in decreased rotational constants. This also explains the success of the simple model.

4.1. *Monomers*

Rotational spectra of a few single-molecule very light rotors (with rotational constants larger than $5\,cm^{-1}$) have been measured in helium nanodroplets: HF [181], H_2O [182], NH_3 [183,184], and CH_4 [185]. For these molecules, the rotational constants in the gas phase are larger than in helium nanodroplets by 1.6%, 3%, 5%, and 4.5%, respectively. The recent measurement for NH_3 by Slipchenko and Vilesov [184] brought the reduction of B for this system to the expected range, as the older measurement by Behrens *et al.* [183] gave a surprisingly large ratio of 33%. Apparently, no quantum mechanical calculations of the rotational constants in helium have been performed for these systems, although very accurate *ab initio* He–molecule potentials are available for all of them [186–189] and quantum MC calculations for some of these systems have been published: HF–He_n was investigated by Blume *et al.* [190] and, very recently, Viel *et al.* [191] performed DMC calculations on NH_3–He_n clusters. In contrast, heavier single-molecule rotors, for which the rotational constants decrease by a factor of 3 or so, have attracted a lot of attention. For such systems, measurements have been done both in helium nanodroplets and in large, size-controlled clusters. For several of these systems, mainly those which are linear molecules, quantum MC calculations have been performed. For some molecules, the shifts of the rovibrational transitions due to the helium environment have also been measured and computed. All molecules treated both by theory and experiment will be discussed below. In some cases, the initial theoretical estimates of the behaviour of rotational constants were in disagreement with experiments. So far, such problems have been traced down to insufficiently accurate intermolecular potentials used in the calculations.

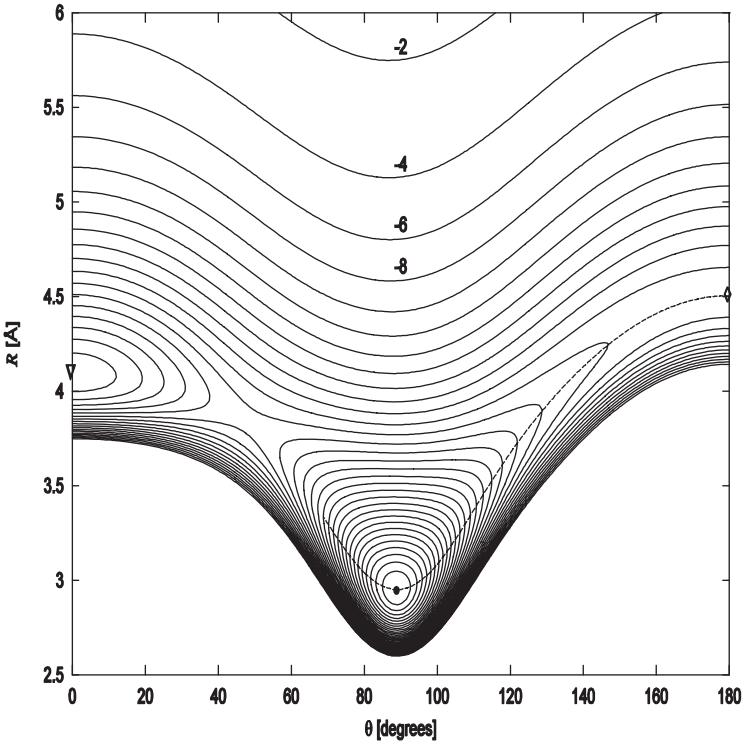

Figure 2. Potential energy surface for He–N_2O [192]. R is the distance between He and the centre of mass of N_2O and the angle $\theta = 0$ corresponds to the configuration He–ONN. The energies are in cm^{-1}.

4.1.1. *N_2O and CO_2: interpretation of experiments based on topology of potentials*

One of the more intriguing experimental findings in measurements of rotational constants in helium nanodroplets was the different extent of the reduction of B for CO_2 and N_2O. Nauta and Miller [47] obtained the infrared spectra of these two molecules and observed, unexpectedly, that the rotational constant of N_2O in helium nanodroplets was half that of CO_2, while in the gas phase these constants are similar. This result was unexpected since due to the similarities of the molecules (N_2O and CO_2 are isoelectronic, linear, of similar lengths, possess zero or nearly zero dipole moments, and have similar values of quadrupole moments and dipole–dipole polarizabilities), their interactions with helium were presumed to be nearly the same. Lacking an accurate potential surface for He–N_2O, Nauta and Miller were unable to explain their findings. One should also point out that the factor of 5.8 decrease observed for N_2O [47] is one of the largest decreases of the rotational constant between the gas phase and helium-nanodroplet values observed for any molecule. Thus, it would be important to understand what features of the potential energy surfaces lead to these extreme cases.

To resolve this problem, SAPT calculations were performed by Chang *et al*. [192] to determine a two-dimensional potential for He–N_2O. The *ab initio* interaction energies were fitted to an analytic function. The resulting fit is shown in Figure 2. Rovibrational energy levels of He–N_2O were then computed [192] on the SAPT surface. At the time

the calculations were performed, no measurements of He–N_2O spectra were available, but such measurements were performed in parallel by Tang and McKellar [193]. The theoretical and experimental spectra agreed very well, with discrepancies typically of the order of $0.01\,cm^{-1}$. Later, He–N_2O potentials were calculated at the CCSD(T) level by Zhou and Xie [194] and by Song *et al.* [195]. The two new potential surfaces, as well as the spectra computed from these surfaces, were very close to those obtained by Chang *et al.* [192]. More recently, Zhou *et al.* [196] obtained a three-dimensional potential for He–N_2O, choosing as the third dimension one of the normal vibrational coordinates of the isolated N_2O molecule. Chang *et al.* [192] also performed some single-point calculations for the He–CO_2 dimer in order to compare the two potentials at the same level of theory and basis set completeness. These results agreed reasonably well with literature *ab initio* He–CO_2 potentials [197–199].

The comparisons of the SAPT interaction energies for He–N_2O with those for He–CO_2 [192] have shown that despite the similarities discussed above, the former interaction is quite significantly, about 30%, stronger than the latter. The physical origins of this difference were elucidated [192] using the SAPT decomposition of the interaction energies. Also the rovibrational states of He–N_2O were compared with those of He–CO_2. This greater potential depth qualitatively explains the greater reduction of the N_2O rotational constant than that of CO_2 in helium nanodroplets since a stronger interaction results in a greater probability of helium atoms sticking to the impurity.

In order to get more insight into the issue of the attachment of helium atoms to N_2O and CO_2, Chang *et al.* [192] found the minimum structures for He_n–N_2O and He_n–CO_2 clusters up to $n=9$ and computed the rotational constants for these structures. For $n=1$ to 6, the constants were steadily decreasing from their gas phase values of 0.42 and $0.39\,cm^{-1}$ to 0.09 and $0.08\,cm^{-1}$, respectively, at $n=6$ (the cluster constants have been scaled for the effects of anharmonicity, i.e. the radius of the ring was increased by the ratio of the average and minimum separations in the dimer). The constants for both molecules remained close to each other at each n. This behaviour can be expected based on the topology of the potentials with the minimum at near T-shaped configuration. Thus, in three-dimensional space, there is a circle of minimum potential equatorial to the molecule. With the minimum separation of 3.0 Å for both dimers and the 3.0 Å minimum separation for He–He, there is enough space on the circle to place up to six helium atoms there. Thus, the potential topology leads to the similarity of the rotational constants in the range $n=1$ to 6. The resulting ring (also called a belt, donut, or doughnut) of helium atoms is characteristic for many linear triatomic or larger molecules since the global minima of the He–molecule potentials tend to lie in this region. The spectra of He_n–N_2O have been measured by Xu *et al.* [200] in parallel with the work of Chang *et al.* [192] and the spectra of He_n–CO_2 some time later [201,202]. The experiments have found the same near equality of the constants up to $n=5$ as predicted by theory [192]. For $n=6$, the experimental values were 0.09 and $0.13\,cm^{-1}$ [200,201], respectively. Thus, the simple method of Ref. [192] agreed very well with experiment for N_2O, but worse for CO_2. In the latter case, however, the theoretical values agree well with experiment up to $n=5$ (at this size, the theoretical constant is $0.10\,cm^{-1}$ and experimental $0.11\,cm^{-1}$), but then the experimental constant increases between $n=5$ and 6, while the theoretical one continues to decrease. This comparison shows that the weaker CO_2 potential cannot hold six helium atoms in the ring. In a dynamic picture, a too weak potential results in a smaller probability of clusters

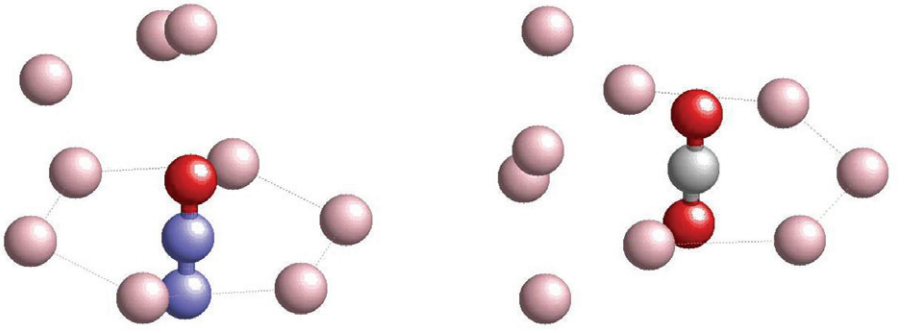

Figure 3. [Colour online] Minimum structures of He_9–N_2O (left) and He_9–CO_2 clusters [192].

beyond some n being formed and surviving, i.e. in a lesser amount of adiabatic following. Whereas simple theory cannot predict a priori at what n this happens, the knowledge acquired from the behaviour of N_2O and CO_2 can be applied in future to other systems of this type.

The analysis of the minimum structures of the clusters with n up to six does not provide any better theoretical explanation of the differences between the B values of N_2O and CO_2 in the nanodroplets than the general statement given above. However, some more clues on the origins of this difference come from considerations of minimum structures of somewhat large clusters [192]. For N_2O, the value of B computed at $n=6$ is very close to that measured in helium nanodroplets ($0.07\,cm^{-1}$ [47]), whereas for CO_2 it is almost a factor of 2 too small (the nanodroplet value is $0.15\,cm^{-1}$ [47]). In the simple theoretical approach, the further addition of helium atoms up to $n=9$ lead to further decreases of B for both systems, but the rate of decrease is much smaller than in the range $n=1$ to 6. For N_2O, this finding agrees reasonably with experimental observations [200] which have found a nearly constant B in the range $n=6$ to 9. However, for CO_2 the experiments have found [201,202] that the rotational constant actually starts to increase from $n=6$ and becomes larger than the nanodroplet value at $n=8$. The reasons for this different behaviour can be understood by analysing Figure 3 adapted from Ref. [192]. As one can see, for N_2O the additional helium atoms tend to gather at the O end of the molecule, where there is a fairly deep secondary minimum [192]. Thus, these atoms do not interact with the atoms of the ring. This minimum should be deep enough to keep a helium atom rotating with the molecule and in this way decreasing the rotational constant. In contrast, since the two secondary linear minima are weak in the case of CO_2, the additional helium atoms aggregate in the ring region. These atoms are too weakly bound to rotate with the molecule and by colliding with atoms of the ring tend to displace the latter out of the ring, which leads to a reduction of the rotational constant upon the increase of n. The atoms that are unable to rotate with the molecule form a 'solvent' within which a He_m–molecule cluster, with $m < n$, freely rotates, which is reminiscent of superfluidity. From this analysis, one can conclude that it is not only the strength of the He–N_2O interaction but also the shape of the potential surface with the two fairly deep minima that combine together to produce one of the largest reductions of B between the gas phase and the nanodroplets. One should emphasize that although the minimizations of

molecule–He_n potentials resulting in static structures such as presented in Figure 3 are useful to gain some insight into the behaviour of a given system, the dynamics of such a cluster involves long-range motions of helium atoms. However, if the probability density resulting from quantum MC calculations is plotted around an impurity, the high-density regions approximately correspond to the potential minima.

One can summarize this discussion by stating that a careful analysis of accurate potential energy surfaces of He_n–N_2O and He_n–CO_2 clusters provides quite a convincing rationalization of the differences in the reduction of the rotational constants for the two molecules. Two factors contribute to the larger reduction in the case of N_2O: about 30% deeper potential well and the shape of the potential energy surface in the region of the secondary minimum. These explanations are confirmed by quantum MC calculations which will be discussed in the next subsection.

The spectra of a system consisting of a linear molecule and an equatorial ring of helium atoms should include the so-called Q branches resulting from rotations around the symmetry axis. Such branches are not observed for most linear molecules in helium nanodroplets. Within the simple model, one can explain this fact as resulting from the symmetry of the system [180,203]. Quantum MC calculations provide a different explanation: the helium atoms show a superfluid response to rotations around the molecular axis, see the next subsection.

The beam experiments have been carried also for larger clusters, up to $n = 80$ for He_n–N_2O [25] and up to $n = 20$ for He_n–CO_2 [201,202]. In the former case, it was found that the constant eventually turns up at $n = 11$, similarly as in the case of CO_2 at $n = 6$. For larger n, B of He_n–N_2O oscillates with n at about 20–50% above the droplet value [25]. This behaviour will be further discussed below. In the range available for He_n–CO_2 [201,202], a similar oscillatory dependence is also visible.

4.1.2. *N_2O and CO_2: interpretation of experiments based on quantum MC calculations*

In order to move beyond the simple model, one has to perform quantum mechanical calculations for He_n–molecule complexes using He–He and molecule–He potentials. The first such calculations had already been done in the mid-1990s [204,205]. This type of calculation has been reviewed in Refs. [40,41,206]. Quantum MC calculations for He_n–N_2O and He_n–CO_2 clusters have been performed in Refs. [207] and [29,202], respectively. The predictions of the rotational constants are not straightforward for the MC-type approaches used so far since such approaches normally reproduce only the ground state properties of investigated systems, whereas the constants are the measure of rotational excitations, i.e. require the knowledge of excited state energies. For quasi-rigid bodies, one can estimate the rotational constants from the average moments of inertia calculated from ground-state wavefunctions, but this method obviously cannot be used for He_n–molecule clusters when only some helium atoms participate in the rotational motions. In fact, such rotational constants, if computed, would offer little improvement over those from the simple minimization method described above. Several extensions of quantum MC methods have been proposed which allow calculations of rotational constants. One approach is to perform fixed-node DMC calculations [40], with nodes corresponding to the first excited rotational state. Another approach, used in RQMC work, utilizes the fact that in the DMC method, as the wavefunction is propagated in imaginary time τ, although it converges to the ground-state wavefunction, contributions

from excited states are contained in the wavefunction for finite τ's. The lowest excitation energies can be extracted from multipole autocorrelation functions in τ by fitting these functions with a sum of exponentials of excitation energies [208]. A different method, involving integral transforms [174], is used in POITSE work, however, the method of the multiexponential fit can also be applied there. These two methods were compared in the case of He_n–N_2O clusters by Paesani and Whaley [207] (within the POITSE approach) and agreed to 2–3 significant digits in rotational energy levels.

Paesani and Whaley [207] performed extensive calculations for He_n–N_2O applying several MC methods: VMC, DMC, PIMC, and utilizing the He–N_2O potential of Chang *et al.* [192]. In general, their findings about ground-state configurations confirmed those of Chang *et al.* [192] discussed above. One important exception is that already at $n=6$ one of the helium atoms is most likely found in the secondary minimum rather than in the ring. However, starting with $n=8$, the ring does contain six atoms, as shown in Figure 3. The rotational constants, computed in Ref. [207] for $n=1$ to 16, agreed fairly well with the measured values [200] available at that time up to $n=12$. Later, the rotational constants were measured also for larger n [25] and the calculations of Ref. [207] predicted the opposite trend in the range $n=13$ to 16 than found experimentally.

The PIMC calculations of Ref. [207] shed light on superfluid properties of the clusters. It has been found that the atoms in the ring exhibit superfluid response starting from $n=5$, but only for the motions around the molecular axis. The superfluid fraction for such motions, denoted in Ref. [207] as $f_{\parallel}^{s}$, changes from 0.05 for $n=4$ to 0.9 for $n=5$. It is important to realize that the motions are cyclic permutation exchanges which do not correspond to rotations of the ring around the molecular axis [29]. Thus, there is no angular momentum projection along the molecular axis and the rotational spectra are characteristic for a linear rotor. Consequently, the symmetry arguments of the simple model are not needed to explain the non-existence of the Q branches. One may, of course, modify the simple model by assuming that the ring exhibits a superfluid response to rotations around the molecular axis. The findings of Ref. [207] also correlate well with the fact that some Q branches are observed for very small He_n–N_2O clusters, up to $n=6$ [25]. The Q branches have also been observed in nanodroplets for some linear dimers, see Section 4.2.4.

The superfluid fraction is much smaller for the motion along the molecular axis than around it. This quantity, denoted in Ref. [207] as $f_{\perp}^{s}$, is practically zero up to $n=7$ and then increases to about 0.2 [207]. This increase correlates well with the fact that the rotational constant has the lowest value at $n=8$ and it only slightly increases for larger n. One may say that, for larger n, six helium atoms form the ring, $\sim$2 atoms are attached in the region of the secondary minimum near the O end of the molecule, and the remaining atoms form a superfluid solvent which does not rotate with the molecule. The $\sim$8 atoms attached to the molecule are not completely rigid but undergo exchanges with the remaining atoms. The degree of such exchange can vary with n and in the effect the rotational constant continues to change, although not as much as for lower n. One should mention that the analysis of the superfluid behaviour performed in Ref. [207] and described above is possible only assuming that the N_2O molecule is fixed in space. For rotating and translating N_2O, only the total, isotropic estimator of superfluidity is available. This estimator can also be computed for a fixed N_2O and it has been found

to be rather sensitive to this approximation. Thus, the results for the superfluid fraction discussed above probably have large uncertainties. Recently, Xu *et al.* [209] developed a method for PIMC calculations of an estimator of the superfluid fraction which they compare to the $f_{\perp}^{s}$ values of Ref. [207]. In contrast to Ref. [207], the method of Ref. [209] does take into account the motion of N_2O. The superfluid fractions computed in Ref. [209] are dramatically different from those of Ref. [207]: about four times larger in the range of n from 10 to 16.

A similar study of He_n–N_2O clusters was performed by Moroni *et al.* [210] using the He–N_2O potential of Ref. [195] and the He–He potential of Ref. [102]. One can now compare both the calculation of Ref. [207] and that of Ref. [210] with the new measurements carried out by McKellar up to $n = 80$ [25]. This comparison shows that although both calculations predict the general experimental trends in the dependence of B on n reasonably well (except for the predictions of Ref. [207] in the range of n from 12 to 16), the remaining discrepancies with experiment are significant and call for further theoretical effort. Overall, the calculations of Ref. [210] agree with experiment better than those of Ref. [207], which may be partly due to the use of more accurate potentials in the former case. Still, for several values of n, the discrepancies between the predictions of Ref. [210] and experiment are around 10% and at $n = 30$ the discrepancies are as large as 20%. Later calculations by Xu *et al.* [209] using the PIMC method and the same potentials as in Ref. [210] gave results very similar to those of Ref. [210].

Let us analyse what may be the reasons for the discrepancies discussed above. Since the He–He potential of Ref. [102] is accurate to better than 1% [102,112] and the He–N_2O potential of Ref. [195] gives the rotational transition energies of He–N_2O which agree with experiment to about 1%, the fairly large discrepancies between experiment [25] and the calculations of Ref. [210] observed for the larger clusters are probably not due to the inaccuracies of the two-body potentials in any significant measure, at least not in the regions near minima. There is a chance that the He–N_2O potential of Ref. [195] is insufficiently accurate at large separations which might explain why the agreement between theory and experiment deteriorates for large clusters. This potential was obtained by interpolation and lacks the correct asymptotics of the potential of Ref. [192]. If this source of errors is small, one should consider the possibilities that the discrepancies are due either to the assumption of rigidity of N_2O or to many-body non-additive effects [115]. The rigidity approximation was investigated by Jeziorska *et al.* [211] on the example of the Ar–HF dimer. It was found that if the HF geometry averaged over the ground-state vibration function – the so-called $\langle r \rangle$ geometry – is used (as was the case in the He–N_2O calculations of Refs. [192,195]), the difference between rigid-monomer and three-dimensional calculations of the dissociation energy of the complex is only 1%. This difference should be even smaller for N_2O since the amplitude of the vibrational motion is much smaller than in the case of HF. Three-dimensional calculations for He–N_2O have in fact been recently performed [196]. The values of the energy the ground rovibrational state of He–N_2O from such calculations are about 1% different from those from the two-dimensional calculations, which is larger than just estimated. However, this is mainly due to the fact that the authors of Ref. [196] used the equilibrium monomer geometry, which leads to much larger errors than the $\langle r \rangle$ geometry (4% in the case of Ar-HF [211]). Thus, the rigidity assumption in the DMC calculations for He_n–N_2O should lead to much smaller

uncertainties than the observed discrepancies between theory and experiment. The other possible source of uncertainties, the pairwise non-additive interaction, should be dominated by three-body effects. The three-body interactions between helium atoms are smaller than the errors of the two-body helium potentials used [161,166]. No calculations have been performed for He_2–N_2O so far. In fact, apparently no data are available on any cluster of this type. Jakowski *et al.* [212] have analysed non-additive effects in He_2–CO_2, but no information about the relative importance of three-body effects can be extracted from their paper. For Ar_2–HF, the three-body non-additive interactions amount to 3.5% of two-body interactions [213] at the minimum configuration. This value is certainly an upper bound for the analogous contribution in He_2–N_2O since the non-additive interactions are relatively more important for polar and polarizable monomers, see Figure 33.1 in Ref. [115]. Even if many-body effects contribute 1–2% to the energies of He_n–N_2O clusters, this would be insufficient to explain the discrepancies between theory and experiment in the rotational constants of the clusters.

In summary, the discussed discrepancies between theory and experiment are probably due only to a small extent to the uncertainties of the potential energy surfaces (except for the possibility of errors resulting from the long-range behaviour of the potential of Ref. [195]) and the reasons for the discrepancies have to be found elsewhere. The analysis performed above indicates also that the differences between the results of Refs. [207] and [210] are probably not entirely due to the use of different potentials. Thus, it would be of importance to perform calculations on He_n–N_2O using the computer codes of these two groups with identical potentials. This would allow one to estimate uncertainties resulting from the use of the DMC approach. One may also compare in the future the energies of rotationally excited state (as this has been already done, e.g. in Refs. [214,215]) rather than the rotational constants. The values of B are obtained from fits to energy levels and these fits can be done in several ways, see the discussion of this issue in Ref. [207].

Quantum MC calculations for He_n–CO_2 have been performed by Tang *et al.* [202] using the He–CO_2 potential of Korona *et al.* [199] and by Paesani and Whaley [29] using the potential of Yan *et al.* [197]. The results of the former calculations are probably somewhat more accurate since these authors used better intermolecular potentials, not only for He–CO_2, but also for He_2 (the potential of Ref. [102] used in Ref. [202] is more accurate than the potential of Ref. [156] used in Ref. [29], cf. Section 3). This is reflected in the better agreement with experiment achieved by Tang *et al.* [202], although in both cases the agreement is good. The computed parallel (motion of helium atoms around the molecular axis) superfluid fraction is a similar function of n as for the He_n–N_2O clusters [29], but the perpendicular (motion of helium atoms along the molecular axis) superfluid fraction is dramatically different: it starts growing already at $n = 6$ and becomes close to one at $n = 12$. This is clearly connected with the relatively weaker binding of helium in the secondary minima of the He–CO_2 potential than of the He–N_2O potential, as found in Ref. [192] and discussed above. Since the helium atoms corresponding to the superfluid density do not rotate with the molecule, there is no contribution of such atoms to the rotational constant B. The large value of the perpendicular superfluid fraction also implies that the atoms from the ring are involved in exchanges along the molecular axis, effectively making the ring smaller, which explains the increase of B for n between 5 and 12.

4.1.3. *OCS*

A similar system to those discussed above are the He_n–OCS clusters [24,208,216–220]. The potential energy surface of He–OCS is fairly similar to that of He–CO_2. The gas-phase rotational constant of OCS is about half that of CO_2 and it becomes reduced by a factor of 2.7 in helium nanodroplets [180], similarly as that of CO_2. This means that more helium atoms have to adiabatically follow the motion of the impurity in the former case, which is possible due to the slower rotation of OCS. This reasoning is well supported by the dependence of B on n for small n. The rotational constant decreases up to $n = 9$ in the case of OCS, to reach a value about 1.7 times smaller than in the droplet, whereas it decreases only up to $n = 5$ to a value 1.4 smaller than in the droplet in the case of CO_2. For larger n, the He_n–OCS constant initially increases which can be interpreted as due to the additional helium atoms disturbing the lower-n structures, as in the cases discussed above. After the value of B approaches the nanodroplet value, it starts to oscillate slightly above this value, and is still about 5% larger at the largest measured value of n equal to 72 [24].

Another well determined characteristics of He_n–OCS clusters is provided by the shifts of the fundamental vibrational frequency of OCS upon complexification. The n-dependence of such shifts was computed prior to any measurements by Paesani *et al.* [217] using the DMC method. The He–OCS potential energy surface dependent on intramonomer vibrational coordinate was developed earlier by Gianturco and Paesani [221] using the so-called DFT-D electronic structure method, i.e. performing DFT supermolecular calculations and supplementing the result with an asymptotic dispersion energy (note that this DFT approach describing the electronic wavefunction in the Born–Oppenheimer approximation should be distinguished from the previously discussed DFT approach applied to describe the wavefunction of helium atoms treated as point particles). Unfortunately, the predicted vibrational shifts were opposite to those measured later by Tang *et al.*, see Figure 2 in Ref. [216]. The reason for the discrepancy was the inaccurate potential energy surface of Ref. [221]. This is not surprising since a DFT-D approach cannot be expected to provide results of near spectroscopic accuracy, as actually was seen by Gianturco and Paesani [221] in comparisons of their spectra of He–OCS with experiment and with calculations of Higgins and Klemperer [222]. Later, an even more accurate He–OCS potential than that of Higgins and Klemperer was obtained by Howson and Hutson [223]. After Paesani and Whaley computed a new potential at the MBPT4 level, theoretical results were brought to excellent agreement with experiment [207].

The potential of Ref. [221] did better in calculations of rotational constants [224], however, it predicted the 'turnaround' of B at $n = 6$, instead at $n = 9$ [24]. In contrast, calculations of Moroni *et al.* [208] with the potential of Ref. [223] gave the turnaround at the correct value of n. For $n \geq 12$, none of the published calculations [208,224–226] predicted reasonably well the experimental dependence measured in 2006 [23], see Figure 2 in Ref. [23]. The best agreement was reached by the calculations of Ref. [208] with the 'morphed' potential of Ref. [223] (i.e. with an originally *ab initio* computed potential adjusted to better reproduce measured spectra of He–OCS), although the same group later advocated [225] to use the 'unmorphed' potential [223]. Thus, an accurate reproduction of experimental trends of $B(n)$ remains an important challenge for theory and may require a further improvement of the interaction potentials involved in quantum

MC calculations. One should also note that the agreement between theory and experiment is significantly worse for OCS than for N_2O.

4.1.4. *HCCCN*

Cyanoacetylene (HCCCN) was investigated in nanodroplets as a model of elongated species [44,45,49,214,227]. A two-dimensional potential energy surface for He–HCCCN was developed by Akin-Ojo *et al*. [203] based on *ab initio* calculations using SAPT and supermolecular methods at various levels of electron correlation. HCCCN was taken to be a rigid linear molecule with the interatomic distances fixed at the experimental 'r_0' geometry extracted from the ground-state rotational constants (the more appropriate $\langle r \rangle$ geometry could not be deduced from available data). An interesting question answered by Ref. [203] concerned the topology of the potential energy surface. Complexes of helium with diatomic molecules containing hydrogen have minima in linear configurations [228], whereas longer linear molecules not containing hydrogen usually have minima in T-shaped configurations. In the case of HCN, an analogue of HCCCN, the position of the minimum was controversial for some time but in 2001 Toczylowski *et al*. [56] performed high-level *ab initio* calculations and found the global minimum in the linear configuration with the depth of $30\,cm^{-1}$ and a local minimum at a bent T-shape geometry with the depth of $22\,cm^{-1}$. The linearity of the minimum structure was later confirmed by experiments [229]. Thus, the topology of the potential energy surface for He–HCCCN was an open question. The complex was found in Ref. [203] to have a global minimum with the depth of $42\,cm^{-1}$ at a near T-shaped configuration and a secondary minimum, $30\,cm^{-1}$ deep, at the linear configuration with the He atom facing the H atom. Rovibrational bound state calculations of spectral transitions and intensities were performed in Ref. [203] for the ^{4}He–HCCCN and ^{3}He–HCCCN complexes. No experimental spectra have been published for He–HCCCN at that time, so theory provided the first characterization of this system. The spectra of He–HCCCN were measured in 2005 by Topic and Jäger [230] and agreed very well with the predictions of Akin-Ojo *et al*. [203]. Topic and Jäger have also performed CCSD(T) calculations for He–HCCCN using much larger basis sets than in Ref. [203], up to augmented quadruple-zeta quality bases supplemented by bond functions, containing 456 functions compared to 185 functions applied in Ref. [203]. Such an increase of the basis size increases the time of calculations at the CCSD(T) level almost 40 times. Despite the significant increase in the size of the basis, the improvement of the agreement with the measured values was fairly small: the average discrepancy of computed and measured energy levels was decreased from 2.1% to 0.6%. This is probably due to two reasons. First, the basis set used in Ref. [203] was optimized for intermolecular interactions. Second, the bond functions were placed in Ref. [203] at such a point that these functions always improve the description of the dispersion interaction whereas in Ref. [230] the functions were placed in the midpoint of the separation between the centres of mass of HCCCN and the helium atom, which results for shorter separations in the bond functions overlapping the HCCCN basis and leading to linear dependencies. Interestingly enough, one of the surfaces obtained in Ref. [203], the SAPT2 surface computed at the level of SAPT approximately equivalent to the supermolecular many-body perturbation theory at the second-order (MBPT2) level, had the average error of only 0.9%. Such a performance of a lower-level method can happen for cases where the perturbation expansion (or the cluster expansion) of the

interaction energies converges in an oscillatory way (see Ref. [231] for several examples of such behaviour). Apparently, Topic and Jäger [230] have not fitted the computed *ab initio* energies by any analytic function. Therefore, they had to compute a large number of points (697) to achieve sufficiently dense covering of the potential surface. In contrast, only 120 points were computed in Ref. [203] and fitted to a physically justified analytic functional form.

The effective rotational constant of HCCCN solvated in a helium droplet was estimated by Akin-Ojo *et al.* [203] by minimizing the energy of He_n–HCCCN for $n = 2 - 12$, selecting the $n = 7$ complex as giving the largest magnitude of the interaction energy per He, and shifting the resulting ring of He atoms to the position corresponding to the average geometry of the ground state of the He–HCCCN dimer. This estimate was within 4.8% of the measured value [44]. Thus, the fact that the decrease of the rotational constant of HCCCN in helium nanodroplets amounts to a factor of 2.9 [45], i.e. is similar to many other molecules with the gas phase rotational constants of a few tenths of a wavenumber, is due to the topology of the potential energy surface of He–HCCCN which leads to the creation of the characteristic equatorial ring. The first experiments on He_n–HCCCN clusters were performed only recently by Topic *et al.* [214] and were accompanied by quantum calculations using RQMC. Both the potential of Topic and Jäger [230] and the potential of Akin-Ojo *et al.* [203] were used in the calculations, the latter one leading to a marginally worse agreement with experiment for small clusters and marginally better agreement for larger clusters. The reason for this relation could be that the potential of Ref. [203] is given in a functional form with the correct asymptotic behaviour for large intermolecular separation. In contrast, the calculations of Ref. [230] apparently have not been fitted and the potential is available only in a tabular form. Note that only the points computed in Ref. [230] at the lower, triple-zeta quality level were used since the quadruple-zeta quality calculations were performed at a reduced number of points. The results of RQMC calculations agreed very well with the analysis of Akin-Ojo *et al.* [203]. In particular, the $n = 7$ cluster was found to have the rotational transition frequency about 20% larger than the droplet value. This agreement indicates that for molecules with as small gas-phase rotational constant as that of HCCCN and with He–dopant interactions in the range of 40–50 cm^{-1}, the adiabatic following is fairly complete. As discussed above, the N_2O molecule belongs to the same category, whereas for CO_2 the adiabatic following is much less complete due to weaker intermolecular interactions. However, static estimates of Ref. [203] for He_n–HCCCN differ from the results of dynamical calculations of Ref. [214] in that the seventh helium atom is already significantly located at the secondary minimum on the H side in the latter approach. The rotational transition frequencies continue to decrease up to $n = 9$ when the helium atoms attach mainly to the secondary minimum, as in the case of N_2O. Then the frequencies increase until $n = 13$ to become about 40% larger than the droplet value. Topic *et al.* [214] have also used PIMC to calculate the superfluid fraction and found that it increases for n between 5 and 13 and then becomes approximately constant. When this fraction is still small, the additional atoms between 6 and 9 continue to be strongly attached to HCCCN and reduce the rotational constant. After the superfluid fraction increases further, not only do the additional atoms become superfluid and do not rotate with the dopant, but some of the previously attached atoms move instantaneously into the superfluid due to exchanges. When the superfluid fraction saturates, the additional atoms start attaching again to HCCCN,

reducing the transition frequency. The oscillatory process continues with the next minimum reached at $n = 22$, close to the complete first solvation with $n \approx 21$ [214].

4.1.5. *CO*

Recently, CO has been added to the list of molecules investigated in size-resolved helium clusters [232–234]. The spectra of this molecule were later measured in helium nanodroplets [235]. These clusters have been investigated in DMC and PIMC calculations [215,226,235–237]. Some of the DMC calculations [238,239] even predate the experiments. Paesani and Gianturco [239] calculated in particular the shifts of the fundamental vibrational transition frequency due to the complexification. The calculations were performed using the SAPT potential of Ref. [240] and a potential developed by the authors using the DFT-D method [239]. For $n = 1$, the shift predicted by the SAPT potential had the same sign as the experimental shift of $-0.026\,\mathrm{cm}^{-1}$ [241] but was about two times too large in magnitude, whereas the shift predicted by the DFT-D potential was of opposite sign. The shifts given by the DFT-D potential were calculated up to $n = 100$ and at this size are of opposite sign and three times larger in magnitude than the experimental value measured later in the droplets by von Haeften *et al*. [235]. The shifts given by the SAPT potential were computed up to $n = 50$ and agree in sign with the droplet experiment but are almost four times too large in magnitude. Vibrational shifts for intermediate size clusters are not available. The discrepancies between theory and experiment could be expected to be due to inaccuracies of the potential energy surfaces, as in the case of the early calculations of the OCS shifts discussed above. Recently, a three-dimensional potential energy surface for He–CO has been calculated by Peterson and McBane at the CCSD(T)/CBS level with a correction for full triple excitations contribution from the CCSDT level of theory [242]. The He–CO rovibrational levels agreed with experiment somewhat better than the levels given by the SAPT potential: the root mean square error with respect to the observed transitions was reduced from $0.04\,\mathrm{cm}^{-1}$ to $0.01\,\mathrm{cm}^{-1}$. In particular, the shift of the fundamental frequency equal to $-0.024\,\mathrm{cm}^{-1}$ agreed very well with experiment. This potential was used by Skrbic *et al*. [215] in RQMC calculations for He_n–CO clusters up to $n = 100$. The vibrational shifts were about two times smaller than those given by the SAPT potential and in particular the values saturated around $n = 20$ at about $-0.4\,\mathrm{cm}^{-1}$, and for n larger than 50 even slightly decreased. At $n = 100$, the theoretical value was about 50% larger than the experimental nanodroplet result. Taking into account that the latter result was estimated [235], the agreement was reasonably good. However, Skrbic *et al*. [215] have found that, due an incorrect asymptotic behaviour of the potential of Ref. [242], the results for larger clusters cannot be trusted. With the correct asymptotic behaviour, the shifts should continue to decrease and saturate only at a larger n, as it is the case for the results obtained with the SAPT potential (which has the correct asymptotic behaviour). Thus, one may expect the discrepancies with experiment to increase when the potential is improved.

4.1.6. *Other monomers*

There were a couple of other single molecules for which both measurements in the helium nanodroplets and theoretical calculations have been performed, but none of

those molecules have also been measured in size-controlled clusters, so that comparisons between theory and experiment are only qualitative.

One molecule in this category which has received significant theoretical attention is HCN. This molecule is an interesting intermediate case between 'light' and 'heavy' rotors, with the rotational constant in gas phase of $1.5\,cm^{-1}$ compared to $20\,cm^{-1}$ for HF, $0.42\,cm^{-1}$ for N_2O, and $0.20\,cm^{-1}$ for OCS. The spectrum of HCN in helium nanodroplets was first measured by Conjusteau *et al.* [243] and a 26% reduction was found. No experiments have been performed for He_n–HCN clusters with controlled n, but nevertheless this system was the subject of two papers presenting quantum MC calculations for such clusters. Paolini *et al.* [225] used RQMC to investigate the clusters with sizes up to $n = 50$. These authors found that the convergence with n to the droplet value is very fast and the droplet limit is reached for n about 15. Similar conclusions were reached by Mikosz *et al.* [244].

The He_n–LiH clusters have been recently investigated using DMC and PIMC by Zillich and Whaley [61]. No measurements have been performed either for these clusters nor for LiH in helium nanodroplets. The reason for the interest in this system is that LiH is a light rotor (the rotational constant is $7.5\,cm^{-1}$ in the gas phase) with a very anisotropic and deep ($-177\,cm^{-1}$ [245]) interaction potential. In consequence, the adiabatic following is strong despite fast rotation [61] and the rotational constant is very significantly, about 16 times, reduced in He_n–LiH clusters. These two systems provide additional examples that the percentage reductions of the rotational constants is mainly due to the details of potential energy surfaces.

All the molecules discussed above were linear. Only very few quantum MC calculations have been published for nonlinear molecules. Sulfur hexafluoride, SF_6, the first molecule whose spectrum was measured in helium nanodroplets, was investigated most often. The pioneering such calculations of Barnett and Whaley, performed using DMC, were published in 1993 [204], followed by the PIMC calculations of Kwon *et al.* [205]. However, no *ab initio* potential energy surface has been developed for He–SF_6. Recently, Kwon *et al.* [246] carried out calculations for He_n–phthalocyanine, a planar conjugated macrocyclic molecule (porphyrin with four extra benzene rings attached). Until recently, calculations of accurate interaction potentials for large polyatomic molecules was outside the range of *ab initio* methods, but the SAPT(DFT) approach [247–250] developed in the past few years can treat such systems (a dimer with 42 atoms has recently been investigated [251]).

4.1.7. *Large clusters vs. nanodroplets*

Very recently, beam experiments were performed on He_n–molecule clusters with a controlled size, containing nearly a hundred helium atoms, in this way reducing the gap between such experiments and measurements made in the smallest helium nanodroplets which contain somewhat less than one thousand atoms. For all of the investigated systems, even at the largest values of n, the properties measured in He_n–molecule clusters were still significantly different from those measured in nanodroplets [23–25,201,202,209,214,234]. These experiments have dramatically changed the previous opinion based on results of quantum MC calculations (done before the cluster experiments started) indicated that the rotational constants saturate at the nanodroplet values already for clusters with less than 10 helium atoms [252]. However, as discussed extensively above, newer

calculations agree with the cluster experiments reasonably well, although the agreement does deteriorate somewhat for larger cluster sizes. One may note that the question of convergence of cluster properties to properties of the bulk is an important and frequently investigated subject in condensed matter physics.

The lack of convergence to the nanodroplet limit even for the clusters size approaching a hundred atoms is surprising since these values correspond to several solvation shells around the impurity. For example, the experiment of McKellar [25] has found that even for $n = 80$, corresponding to about four solvation shells around N_2O, the value of B measured in the He_n–N_2O clusters is 25% larger than the nanodroplet value. Apparently, the addition of further shells is still necessary to make the solvent more tightly bound and develop a stronger 'surface tension' on the surface of the cavity surrounding N_2O, resulting in a smaller number of exchanges with atoms attached to the molecule.

The values of B computed or measured in the clusters show minima near the values of n corresponding to complete shells which allow the most symmetric distribution of helium atoms and therefore best mimic the droplet. This oscillatory behaviour related to the buildup of consecutive solvation shells was investigated for He_n–N_2O by Xu *et al*. [209]. Such behaviour has so far been observed for N_2O, CO_2, OCS, and HCCCN. The degree of oscillations and the overall rate of convergence to the nanodroplet value appears to be strongly dependent on the impurity molecule. For OCS [24], starting from $n = 30$, the values of B oscillate above the nanodroplet value and for $n = 30$–72 are about 5–10% larger than this value, i.e. the convergence is better than for N_2O [25]. Still, the oscillations decay rather slowly for the He_n–OCS clusters and probably many dozens more atoms are needed to get within 1% of the nanodroplet value. The convergence appears to be much faster for light rotors, although experimental cluster data are available only for CO [234]. The values of rotational transitions in He_n–CO clusters converge monotonically to within 5% of the nanodroplet value at the largest value of $n = 50$. Theoretical predictions are in poor agreement with experiment in the range of $n = 20$–50 [215], probably due to the problems of the interaction potentials discussed above. For He_n–HCN, no experimental work has been published. The DMC calculations for this system indicate [225,244] that the convergence to the nanodroplet limit is very fast in this case and the limit is reached with n of about 15.

Without doubt, we will see in the next few years further attempts aimed at closing the gap between the clusters with controlled number of helium atoms and the nanodroplets. Both theory and experiment will be pushed to larger cluster sizes. One may also hope that experiments in nanodroplets can be performed with some control of droplet size. If this size can be reduced to a few hundred helium atoms, most likely the value of B from such experiments will be measurably different from that obtained in experiments on droplets containing a few thousand atoms. At the same time, such size-controlled experiments would allow better 'two-sided' extrapolations in the gap region.

4.2. *Dimers*

The number of molecular clusters (including some atom–molecule clusters) whose spectra have been measured in helium nanodroplets is rather large and some of this work was briefly described in Section 2. All such measurements up to 2001 are listed in Table 1 of Ref. [34], and several more species have been measured since then. However, quantum

MC calculations are much more difficult for such clusters and require, in addition to the He–molecule potential(s), also an appropriate molecule–molecule potential. Whereas experiments were performed on clusters as large as hexamers and heptamers (and signals of clusters with about 15 monomers have been identified in some spectra [253]), theoretical calculations have so far been restricted to dimers. There have been only a handful of such calculations published, and we will briefly discuss all of them below. No experiments have yet been performed on He_n–(molecular–cluster) complexes with a controlled n, so comparisons between theory and experiment can be only qualitative.

4.2.1. $(HF)_2$

The first calculation related to experimental investigations of clusters of molecules embedded in helium nanodroplets was the work of Sarsa *et al*. [254]. These authors applied DMC methods to investigate He_n–$(HF)_2$ with n ranging from 1 to 10. They used a SAPT potential [186] for He–HF interactions and a very accurate $(HF)_2$ potential first fitted to *ab initio* computed interaction energies and then tuned to spectral data by Klopper *et al*. [66]. More extensive calculations with the same potentials were published later by Jiang *et al*. [255]. Hydrogen-bonded dimers exhibit tunnelling of hydrogen atoms between symmetry-equivalent minima, which leads to characteristic tunnelling splittings of spectral lines. Whereas the vibrational spectra of isolated molecules or the monomer's spectra within clusters change little in helium nanodroplets, the much lower-frequency intermonomer vibrations can be expected to change appreciably, and the small tunnelling splittings can be particularly sensitive. Indeed, Nauta and Miller [256] measured the splittings of $(HF)_2$ lines in nanodroplets that were reduced very significantly, to about 40% of the value in the gas phase. Calculations of Sarsa *et al*. [254] have found that the majority of the decrease takes place already for $n=4$. The configuration of the first four helium atoms is similar to that found for linear single molecules, i.e. these atoms form an equatorial ring. Later work [255] has shown that, for larger n, five atoms are included in the ring. The ring is most rigid in the He_5–$(HF)_2$ cluster. The further helium atoms spread along the dimer axis and their quantum exchanges with the atoms of the ring reduce the rigidity of the ring. The presence of the ring can explain in a very simple way the reduction of the tunnelling splitting by helium atoms, as the ring is located 'near' the transition path and therefore interferes with tunnelling (see, however, the discussion of the $(HCl)_2$ case below).

Experiments have also found [256] that the rotational constant A of $(HF)_2$, corresponding to the rotation around the F–F axis, is increased in helium. This is unusual since, as discussed above, the rotational constants tend to decrease in nanodroplets. The simplest way to explain the increase of A is to assume that the presence of the helium atoms changes the geometry of $(HF)_2$. This dimer is significantly nonlinear in the gas phase, with the acceptor monomer bent 68 degrees from the F–F axis [66]. If the dimer becomes more linear in nanodroplets, this would explain the observed change of A. Nauta and Miller [256] considered the increased linearity likely to happen due to the induction interaction of $(HF)_2$ with helium atoms: linear $(HF)_2$ has a larger dipole moment than bent $(HF)_2$ and this leads to larger induction interactions. The induction interactions make indeed a fairly large contribution to the He–HF interaction energy [186]. These interactions are fully included in the potentials used by Sarsa, Jiang, *et al*. [254,255], so that the postulated increased linearity of $(HF)_2$ should be visible in the calculations of Refs. [254,255].

Unfortunately, the trend is just opposite: at $n = 20$, the bending angle increases by 2.5 degrees and also the nonlinearity of the hydrogen bond increases by 1.1 degree, leading to a slightly more nonlinear dimer than the gas-phase one (unpublished data from Ref. [255]). Therefore, the increase of A remains unexplained at the level of two-body potentials, and an important question for future work is whether three-body effects may provide a large enough contribution to the total interaction potential to increase the linearity of $(HF)_2$. As discussed above, in He_n–molecule systems the three-body effects are probably negligible at the current levels of accuracy. Such effects will be larger, however, perhaps as large as a few percent of the two-body interaction energy, in He_n–molecule$_2$ complexes. This is due to the fact that the leading three-body induction mechanism, which is exactly zero in the former case, may become sizable in the latter case. This mechanism is as follows: the permanent multipole moments on monomer A induce multipole moments on monomer B and the latter moments interact with the permanent multipole moments of molecule C. Such interaction is zero for A–B–C = HF–He–He since helium is non-polar, but may be fairly significant for HF–He–HF.

4.2.2. *$(HCl)_2$*

It was natural to extend the investigations of the He_n–$(HF)_2$ clusters to the dimer of HCl. However, no reliable potential surface was available for He–HCl. Therefore, to enable such studies, a two-dimensional intermolecular potential energy surface of the He–HCl complex has been computed [228] using the SAPT approach. The HCl molecule was kept rigid with a bond length equal to the expectation value $\langle r \rangle$ in the ground vibrational state of the isolated HCl. In the region of the minimum, the He–HCl interaction energy was found to be only weakly dependent on the HCl bond length, at least as compared to the case of Ar–HF [211]. This finding can be attributed to the smaller dipole moment of HCl relative to HF and the subsequently smaller induction energy component in the case of HCl. The SAPT potential agrees with the semi-empirical potential of Willey *et al*. [257] in finding that, atypically for rare gas–hydrogen halide complexes including the lighter halide atoms, the global minimum is on the Cl side, with the depth of $32.8\,cm^{-1}$, rather than on the H side, where there is only a local minimum, $30.8\,cm^{-1}$ deep. The ordering of the minima was confirmed by single-point calculations in larger basis sets and complete basis set extrapolations, and also using higher levels of theory. Reference [228] has shown that the opposite findings in calculations of Zhang and Shi [258] were due to the lack of mid-bond functions in their basis set. Despite the closeness in depths of the two linear minima, the existence of a relatively high barrier between them invalidates the assumption of isotropy, a feature of some literature He–HCl potentials. The accuracy of the SAPT potential was tested by performing calculations of rovibrational levels of He–HCl. The transition frequencies obtained were found to be in excellent agreement (to within $0.02\,cm^{-1}$) with the measurements of Lovejoy and Nesbitt [259]. The SAPT potential predicts a dissociation energy of $7.74\,cm^{-1}$, which is probably more accurate than the experimental value of $10.1 \pm 1.2\,cm^{-1}$ [259]. The analysis of the ground-state rovibrational wavefunction shows that the He–HCl configuration is favoured over the He–ClH configuration despite the ordering of minima. This is due to the greater volume of the well in the former case.

The potential of Ref. [228], together with the empirical HCl dimer potential fitted to spectroscopic data in Ref. [260], was used by Jiang *et al*. [255] to investigate He_n–$(HCl)_2$

clusters by performing DMC calculations. The gas-phase tunnelling splitting in $(HCl)_2$ amounts to $15.5\,cm^{-1}$ [261] and is more than 20 times larger than that in $(HF)_2$. In fact, the tunnelling splitting in $(HCl)_2$ is comparable to the energy of the rotational excitation of free HCl. Thus, one would expect only a very small effect of the helium environment on the splitting, similarly as in the case of most large rotational constants. The DMC calculations of Ref. [255] were first performed for $n=0$ and predicted a splitting of $14.9\,cm^{-1}$, in reasonably good agreement with experiment. This splitting was practically unchanged in clusters with n ranging from 1 to 14: the deviation was not larger than $0.2\,cm^{-1}$. Thus, the effects of the helium environment were found even smaller than anticipated. At the same time, the He_n–$(HCl)_2$ clusters exhibit the distribution of helium atoms around the dimer similar as in the case of $(HF)_2$, except that the ring becomes saturated with six helium atoms rather than with five. The smallness of the reduction is apparently due to the tunnelling being so fast in the case of $(HCl)_2$ that there is no adiabatic following of this motion by helium atoms. This dynamic effect is probably the main reason for the differences in the behaviour of the tunnelling splittings between He_n–$(HCl)_2$ and He_n–$(HF)_2$ complexes. However, there are also several small static effects which taken individually are not likely to explain the observations, but acting together in the same direction may have an impact. First, Jiang *et al.* [255] have found that the ring is about 0.5 bohr larger in the case of He_n–$(HCl)_2$ than He_n–$(HF)_2$, so that the helium atoms are slightly further from the tunnelling path in the former case. This is partly balanced by the larger size of the HCl monomer, but still the minimum distance on the tunnelling path between the hydrogen of HX and a helium atom from the ring is about 0.3 bohr larger for HCl. Second, although the ring is similar in both cases, the helium atoms of the ring are about 30% less strongly bound for HCl than for HF. More weakly bound atoms result in less resistance to the tunnelling motions. The third reason is that $(HCl)_2$ is more nonlinear than $(HF)_2$. In consequence, the tunnelling path is shorter in the former case (80 degrees vs. 102 degrees), and therefore chances for interferences with helium atoms are smaller.

Very surprisingly, two recent experiments on $(HCl)_2$ in helium nanodroplets found a substantial reduction of the tunnelling splitting: to 28% [262] and 55% [263] of the gas phase value. One should note that both results are indirect. In particular, the authors of Ref. [263] estimated this splitting from the value measured for the excited vibrational state of HCl. Although the experimental findings differ from each other quite substantially, both measurements indicate that there is a much stronger reduction of the splitting in the droplets than in small He_n–$(HCl)_2$ clusters [255]. One possibility for this difference is a coupling of this transition to collective excitations of helium. Couplings of the rovibrational motions of impurity molecules to collective motions of superfluid helium have been the subject of several recent investigations [30,264,265].

4.2.3. *Clusters containing H_2*

Molecular clusters most often investigated in helium solvent were those that include the hydrogen molecule(s). This is due to the possibility of the existence of superfluidity in para-hydrogen complexes [7,60], see the discussion in Section 2. Since the chromophore molecule used in these experiments so far was OCS, Kwon and Whaley [266] investigated the OCS–H_2–He_{63} cluster using the PIMC method and the OCS–H_2 and OCS–He *ab initio* potentials of Refs. [267] and [222], respectively. However, the He–H_2 interactions

were accounted for only in a very approximate way, as described by an empirical one-dimensional potential of Ref. [268]. Nevertheless, the rotational constant of OCS–H_2 agreed well with those measured by Grebenev *et al*. [269]. The more recent DMC calculations of Paesani and Whaley [270] were performed for He_n–$(H_2)_m$–OCS clusters with m up to 17 and the number of helium atoms up to $n = 128 - m$. These authors calculated the shifts of the fundamental vibrational frequency of OCS upon complexification, the quantity measured in Ref. [7]. *Ab initio* He–OCS [219] and H_2–OCS [270] potentials with explicit dependence on the asymmetric stretch in the OCS molecule have been used. The He–H_2 potential was again taken from Ref. [268]. The H_2–H_2 interactions were approximated by the spherical component only of an empirical potential [271]. Despite the use of such approximate potentials, the agreement of the vibrational shifts with the measured values [7] was very good. Apparently, the investigated phenomenon depends mainly on the OCS–H_2 interaction potential. Indeed, due to stronger interactions of OCS molecules with hydrogen molecules than with helium atoms, all the hydrogen molecules in clusters of the sizes considered are in a direct contact with OCS. An analogous system which could be investigated in helium nanodroplets is CO–$(H_2)_n$. For CO–H_2, very accurate potential energy surfaces have been available [272,273]. The spectra of CO–$(H_2)_n$ clusters have recently been measured [274] and DMC calculations performed [274]. Similarly as in the clusters with helium [232], the spectra of CO in hydrogen are significantly more complicated than those of longer linear molecules. Also HF–$(H_2)_n$ complexes have been investigated in helium nanodroplets [275–277]. DMC calculations have been performed for HF–$(H_2)_n$ clusters by Bacic *et al*. [278,279].

4.2.4. *Dimers of HCCCN and HCN*

Recently, Paesani *et al*. [280] published a paper presenting a joint experimental and theoretical investigation of the HCCCN complex with HCN in helium environment. According to *ab initio* calculations of Ref. [280], there are two minima on the dimer surface: the HCN–HCCCN configuration (where the HCCCN monomer is the hydrogen donor in the bond) and the HCCCN–HCN one (with roles reversed). The former dimer exhibited typical spectra of linear molecules that have T-shaped minima in the interaction potentials with helium. Spectra of such systems in helium nanodroplets, despite the existence of an equatorial helium ring around the molecule, do not include the Q branches, as discussed above. However, a Q branch was observed by Paesani *et al*. [280] in the spectrum that has been identified as due to the HCCCN–HCN dimer. This might indicate that this complex is nonlinear in helium nanodroplets. However, the geometry optimizations for the dimer performed by Duberly *et al*. [281] at the MBPT2 level in an augmented double-zeta quality basis set found only minima at linear configurations (actually, the HCN–HCCCN minimum was somewhat nonlinear, see Figure 1 in Ref. [281]). Since the potential was found to be strongly anisotropic in angular coordinates, the authors of Ref. [280] concluded that both dimers remain in linear configurations in helium nanodroplets. Assuming the dimers as rigid molecules in the two linear configurations, Paesani *et al*. [280] computed in each case the dimer–He potentials at the same level of theory as in Ref. [281] and used these potentials in PIMC calculations with up to 200 helium atoms. They found that the non-superfluid densities of helium were quite different in the two cases (notice that the captions of Figs. 10 and 11 in Ref. [280] should say 'non-superfluid' rather than 'superfluid' density [282]). In particular, a large non-superfluid density was

found around the HC end of the HCCCN–HCN dimer, i.e. a number of helium atoms stuck to this end of the dimer. Paesani *et al*. [280] attributed the appearance of the *Q* branch to this density.

The *Q* branches were observed earlier for $(HCN)_n$, $n = 3$, 4, clusters in helium nanodroplets [283]. The PIMC calculations have reproduced the observations very well. The physical interpretations of the PIMC results was that the *Q* branches correspond to unique thermal excitations in the first solvation layer.

4.3. *Trimers and larger clusters*

As discussed in Section 2, several clusters larger than dimers have been observed in helium nanodroplets. No quantum MC calculations have been performed so far for such clusters with the exception of the already discussed clusters involving the hydrogen molecules which, however, play more of the role of a solvent. There are several systems for which there exist potentials enabling such calculations; one example are the Ar_n–HF clusters observed in helium nanodroplets [185]. Several accurate Ar–HF [211,284,285] and Ar–Ar [125] potentials have been published. Even the three-body potentials, very relevant for systems of this type, are available for Ar_3 [168,169,286] and for Ar_2–HF [213,287,288].

Although calculations of nuclear dynamics for clusters containing more than a pair of molecules have not yet been performed, electronic structure calculations have been used to interpret experiments on such systems. This was mainly done by comparing minimum geometries of various complexes and by calculations the harmonic vibrational transition frequencies. For example, Burnham *et al*. [289] used several empirical and *ab initio* water potentials as well as the MBPT2 method to investigate the energetics of small cyclic water clusters, such as detected in the experiment of Ref. [46]. The main question to be answered was the placement of the water molecule added to a ring of *n* water molecules. One might expect to find this monomer attached to the existing *n*-mer ring. However, all the clusters observed are cyclic, suggesting that the barriers for insertion of one extra water molecule into the ring are very small. Indeed, small barriers have been found for such processes in theoretical studies of Ref. [289]. This analysis could now be made more precise using the recent very accurate potential for water [290]. In contrast to the water clusters, after the cyclic $(HF)_4$ is formed in helium nanodroplets, the fifth monomer does attach to the ring [291]. This finding was also supported by an *ab initio* analysis [291].

4.4. *Metallic clusters*

As mentioned earlier, metal clusters are among systems most often investigated by helium-nanodroplet spectroscopy and it is important to know in the experiments whether such clusters reside on the surface or inside a droplet [36,68,77–88]. This behaviour depends on the strength of the He–metal interaction relative to the He–He interaction. As discussed above, the later value is now known very accurately and amounts to $7.6495\,cm^{-1}$ [112]. Accurate calculations have been recently performed for He–Mg interactions [231] using the CCSD(T) method with all electrons correlated and the FCI method with frozen core. Large basis sets were used and the results were extrapolated to CBS limits. The final estimate [231] of the interaction energy at 5.0 Å was

$-5.11 \pm 0.11\,\mathrm{cm}^{-1}$ including the relativistic correction of $-0.01\,\mathrm{cm}^{-1}$ computed at the CCSD(T) level using the Douglas–Kroll Hamiltonian [292]. This result agrees very well with earlier work by Hinde [293] who obtained an interaction energy of $-4.97 \pm 0.06\,\mathrm{cm}^{-1}$ at the same distance. The actual value of the minimum separation is 5.1 Å and therefore the D_e of the He–Mg potential is $-5.14\,\mathrm{cm}^{-1}$ (obtained by scaling of the value from Ref. [293]). This slightly deeper potential well [231] reinforces the analysis of Hinde [293] indicating that Mg should indeed dissolve in the helium droplets, as found experimentally [86]. As discussed earlier, alkaline earth metals may provide an important probe of ^{3}He–^{4}He mixtures [91].

5. Summary

The method of high-resolution spectroscopic measurements in helium nanodroplets developed about 15 years ago has led to significant discoveries in physics and chemistry. This method enabled studies of superfluid helium with unprecedented precision, yielding insights into superfluidity at the nanoscale level. It also made possible investigations of reactive and fragile molecules that could not be examined in other ways.

The better understanding of superfluidity on microscopic scale was made possible due to synergistic coupling of high-resolution spectroscopic measurements with high-accuracy quantum calculations on helium clusters containing impurities. Calculations for pure helium, both clusters and bulk, predate the helium-nanodroplet developments. To interpret the results of calculations in terms of bulk phenomena such as superfluidity and in terms of quantum ideal gas concepts such as Bose–Einstein condensation, some definitions had to be assumed on the microscopic level and the validity of these assumptions was subject of debate. The same DMC and PIMC simulation techniques have been applied in recent years to helium nanodroplets containing impurities. The good agreement of the predictions from these calculations with high-resolution spectroscopic measurements in helium nanodroplets, both in quantitative and interpretative sense, has greatly increased our confidence in the microscopic description of low-temperature helium resulting from computer simulations. In particular, one can now assume that the questions of the microscopic origins of the behaviour of superfluid helium is resolved. The London–Landau controversy regarding the role of Bose–Einstein condensation is settled with both points of view being partially right, with Landau's opinion closer to the truth as even at $T = 0\,\mathrm{K}$ less than 10% of helium is in the form of the condensate, whereas it is 100% superfluid [176]. More recent calculations predict an even lower condensate fraction, for example $6.9 \pm 0.5\%$ in Ref. [177] and about 8% in Ref. [179].

The spectra of small molecules embedded in helium clusters can be quantitatively predicted by quantum calculations using methods such as DMC or PIMC, provided that high-accuracy helium–molecule potentials are available. The calculations can be made for clusters which are large enough to give spectra that are fairly close to those observed in the droplets. Thus, theory may be used to predict results of measurements in the nanodroplets prior to experiments, and in fact several such calculations have been published, as discussed above. However, the most important experiments from the theoretical viewpoint are the very recent ones on doped helium clusters of controllable size. These experiments enable the most precise comparisons of theory with experiment since such comparisons can be made on identical systems. As the number of helium atoms in the most recent such experiments approached one hundred, the gap

between clusters and nanodroplets may soon be closed. This would be very important not only for understanding superfluidity, but also for understanding the crossover from clusters to condensed phase.

This review has stressed that ultimately the intermolecular interaction potentials decide about the properties of molecules embedded in helium nanodroplets. A good illustration of this fact is that the reductions of the rotational constants due to the droplet environment depend rather critically on the potentials, as discussed here. Furthermore, results of quantum MC calculations depend significantly on the accuracy of intermolecular potentials. Several literature examples have been given showing that inaccurate potentials can lead to qualitatively wrong predictions. Fortunately, with recent developments in computer software and hardware, it is now possible to compute near spectroscopic accuracy potentials for systems as large as the water dimer [290,294,295], and reasonably accurate ones for dimers containing about fifty atoms [251]. In fact, for most of the molecules investigated in helium clusters with controlled size and in helium nanodroplets, the two-body potentials accurate to about one percent or better can be obtained fairly routinely. The errors due to uncertainties of such potentials are currently smaller than the typical discrepancies between quantum MC calculations and experiments. As analysed here, in some cases, in order to further improve the accuracy of theoretical predictions, one will have to consider three-body contributions to interaction potentials. These contributions are much more difficult to compute than two-body ones and pose an important challenge for electronic structure theory. On the other hand, some of the current discrepancies between results of quantum MC calculations and experimental data may also be due to inaccuracies introduced by approximations made in the treatment of the excited rotational states.

In calculations for impurity–He_n clusters, one also needs a He–He potential. Surprisingly, many recently published quantum MC calculations on such clusters or on bulk helium still use older empirical potentials (see also a discussion of the potentials used in a recent review by Barranco *et al*. [41]) such as that of Aziz *et al*. [155,156], whereas in the thermodynamics community it has been recognized since the mid-1990s that *ab initio* potentials had become more accurate, see, e.g. the papers by Aziz *et al*. [154,296]. One often used *ab initio* potential for helium was developed by Korona *et al*. [102] about a decade ago. Very recently a similar but much more accurate potential was published by Jeziorska *et al*. [112]. The use of the latter potential, together with the three-body non-additive potential of Ref. [146], may remove some existing discrepancies between theory and experiment for bulk helium.

Superfluid helium nanodroplets made it possible to form and spectroscopically probe a wide range of species that could not be investigated by any other techniques. These species include atomic and molecular clusters in unusual conformations and states, radicals, and complexes formed in prereactive channels of chemical processes. The new technique allowed also measurements of spectra of several compounds – including biomolecules, semiconductor clusters, and salts – which could not be measured in gas phase or could only be measured with a much lower precision. In addition, the low temperature of the nanodroplets results in considerable simplifications of the spectra of large molecules and therefore one may expect a significant role of these techniques in investigations of biomolecules. One may also expect many important discoveries concerning the creation of novel species, in particular of exotic nanostructures with atoms of various

types layered in some prescribed fashion. The very low temperature of the droplets leads to a significant slowdown of chemical processes and therefore one may anticipate important studies of chemical dynamics using various types of pump-probe time-resolved experiments.

Acknowledgements

This work was supported by the National Science Foundation grant CHE-0555979. The author thanks Drs. J. Peter Toennies and Saverio Moroni for comments on the manuscript.

References

[1] P. Kapitza, Nature **141**, 74 (1938).
[2] J. F. Allen and A. D. Misener, Nature **141**,75 (1938).
[3] A. J. Leggett, Rev. Mod. Phys. **71**, S318 (1999).
[4] L. Landau, J. Phys. (USSR) **5**, 71 (1941).
[5] R. P. Feynman and M. Cohen, Phys. Rev. **102**, 1189 (1956).
[6] C. Kittel and H. Kroemer, *Thermal Physics*, 2nd ed. (Freeman, New York, 1980), pp. 212–214.
[7] S. Grebenev, B. Sartakov, J. P. Toennies, *et al*., Science **289**, 1532 (2000).
[8] D. J. Dean and M. Hjorth-Jensen, Rev. Mod. Phys. **75**, 607 (2003).
[9] A. Einstein, Sitzungsber. K. Preuss. Akad. Wiss., pp. 261–267 (1924).
[10] A. Einstein, Sitzungsber. K. Preuss. Akad. Wiss., pp. 3–14 (1925).
[11] S. N. Bose, Z. Phys. **26**, 178 (1924).
[12] F. London, Nature **141**, 643 (1938).
[13] S. Balibar, J. Low Temp. Phys. **146**, 441 (2007).
[14] M. H. Anderson, J. R. Enshner, M. R. Matthews, *et al*., Science **269**, 198 (1995).
[15] K. B. Davis, M.-O. Mewes, M. R. Andrews, *et al*., Phys. Rev. Lett. **75**, 3969 (1995).
[16] C. C. Bradley, C. A. Sackett, J. J. Tollett, *et al*., Phys. Rev. Lett. **75**, 1687 (1995).
[17] M.-O. Mewes, M. R. Andrews, N. J. van Druten, *et al*., Phys. Rev. Lett. **77**, 998 (1996).
[18] S. Goyal, D. L. Schutt, and G. Scoles, Phys. Rev. Lett. **69**, 933 (1992).
[19] M. Hartmann, R. E. Miller, J. P. Toennies, *et al*., Phys. Rev. Lett. **75**, 1566 (1995).
[20] H. Kamerlingh-Onnes, Commun. Phys. Lab. Univ. Leiden **105**, 744 (1908).
[21] E. W. Becker, Z. Phys. D **3**, 101 (1986).
[22] A. Scheidemann, J. P. Toennies, and J. A. Northby, Phys. Rev. Lett. **64**, 1899 (1990).
[23] A. R. W. McKellar, Y. J. Xu, and W. Jäger, Phys. Rev. Lett. **97**, 183401 (2006).
[24] A. R. W. McKellar, Y. J. Xu, and W. Jäger, J. Phys. Chem. A, **111**, 7329 (2007).
[25] A. R. W. McKellar, J. Chem. Phys. **127**, 044315 (2007).
[26] S. Grebenev, J. P. Toennies, and A. F. Vilesov, Science **279**, 2083 (1998).
[27] P. Sindzingre, M. L. Klein, and D. M. Ceperley, Phys. Rev. Lett. **63**, 1601 (1989).
[28] E. L. Andronikashvili, J. Phys. (USSR) **10**, 201 (1946).
[29] F. Paesani, Y. Kwon, and K. B. Whaley, Phys. Rev. Lett. **94**, 153401 (2005).
[30] R. Lehnig, N. V. Blinov, and W. Jäger, J. Chem. Phys. **127**, 241101 (2007).
[31] E. Loginov, D. Rossi, and M. Drabbels, Phys. Rev. Lett. **95**, 163401 (2005).
[32] V. Mozhayskiy, M. N. Slipchenko, V. K. Adamchuk, *et al*., J. Chem. Phys. **127**, 094701 (2007).
[33] J. P. Toennies and A. F. Vilesov, Ann. Rev. Phys. Chem. **49**, 1 (1998).
[34] C. Callegari, K. K. Lehmann, R. Schmied, *et al*., J. Chem. Phys. **115**, 10090 (2001).
[35] J. A. Northby, J. Chem. Phys. **115**, 10065 (2001).
[36] F. Stienkemeier and A. F. Vilesov, J. Chem. Phys. **115**, 10119 (2001).

[37] J. P. Toennies and A. F. Vilesov, Angew. Chem. Int. Ed. **43**, 2622 (2004).
[38] M. Y. Choi, G. E. Douberly, T. M. Falconer, *et al*., Int. Rev. Phys. Chem. **25**, 15 (2006).
[39] F. Stienkemeier and K. K. Lehmann, J. Phys. B **39**, R127 (2006).
[40] Y. Kwon, P. Huang, M. V. Patel, *et al*., J. Chem. Phys. **113**, 6469 (2000).
[41] M. Barranco, R. Guardiola, S. Hernandez, *et al*., J. Low Temp. Phys. **142**, 1 (2006).
[42] M. Hartmann, N. Portner, B. Sartakov, *et al*., J. Chem. Phys. **110**, 5109 (1999).
[43] J. Harms, M. Hartmann, B. Sartakov, *et al*., J. Chem. Phys. **110**, 5124 (1999).
[44] C. Callegari, I. Reinhard, K. K. Lehmann, *et al*., J. Chem. Phys. **113**, 4636 (2000).
[45] C. Callegari, A. Conjusteau, I. Reinhard, *et al*., J. Chem. Phys. **113**, 10535 (2000).
[46] K. Nauta and R. E. Miller, Science **287**, 293 (2000).
[47] K. Nauta and R. E. Miller, J. Chem. Phys. **115**, 10254 (2001).
[48] K. Nauta and R. E. Miller, J. Chem. Phys. **117**, 4846 (2002).
[49] J. M. Merritt, G. E. Douberly, and R. E. Miller, J. Chem. Phys. **121**, 1309 (2004).
[50] R. Schmied, P. Carcabal, A. M. Dokter, *et al*., J. Chem. Phys. **121**, 2701 (2004).
[51] G. E. Douberly and R. E. Miller, J. Chem. Phys. **122**, 024306 (2005).
[52] C. M. Lindsay and R. E. Miller, J. Chem. Phys. **122**, 104306 (2005).
[53] I. Scheele, A. Conjusteau, C. Callegari, *et al*., J. Chem. Phys. **122**, 104307 (2005).
[54] K. K. Lehmann, J. Chem. Phys. **119**, 3336 (2003).
[55] K. K. Lehmann and A. M. Dokter, Phys. Rev. Lett. **92**, 173401 (2004).
[56] R. R. Toczylowski, F. Doloresco, and S. M. Cybulski, J. Chem. Phys. **114**, 851 (2001).
[57] G. Murdachaew, A. J. Misquitta, R. Bukowski, *et al*., J. Chem. Phys. **114**, 764 (2001).
[58] M. Hartmann, F. Mielke, J. P. Toennies, *et al*., Phys. Rev. Lett. **76**, 4560 (1996).
[59] S. Grebenev, M. Hartmann, A. Lindinger, *et al*., Physica B **280**, 65 (2000).
[60] Y. Kwon and K. B. Whaley, Phys. Rev. Lett. **89**, 273401 (2002).
[61] R. E. Zillich and K. B. Whaley, J. Phys. Chem. A **111**, 7489 (2007).
[62] M. Hartmann, R. E. Miller, J. P. Toennies, *et al*., Science **272**, 1631 (1996).
[63] K. Nauta and R. E. Miller, Science **283**, 1895 (1999).
[64] K. Nauta and R. E. Miller, J. Chem. Phys. **115**, 10138 (2001).
[65] E. M. Cabaleiro-Lago and M. A. Rios, J. Chem. Phys. **108**, 3598 (1998).
[66] W. Klopper, M. Quack, and M. A. Suhm, J. Chem. Phys. **108**, 10096 (1998).
[67] J. Küpper and J. M. Merritt, Int. Rev. Phys. Chem. **26**, 249 (2007); Corrigendum: **26**, 288 (2007).
[68] J. Higgins, C. Callegari, J. Reho, *et al*., Science **273**, 629 (1996).
[69] E. Lungovoi, J. P. Toennies, and A. F. Vilesov, J. Chem. Phys. **112**, 8217 (2000).
[70] A. Braun and M. Drabbels, Phys. Rev. Lett. **93**, 253401 (2004).
[71] A. Lindinger, J. P. Toennies, and A. F. Vilesov, J. Chem. Phys. **110**, 1429 (1999).
[72] A. Lindinger, E. Lugovoj, J. P. Toennies *et al*., Zeitschrift Phys. Chem. Intern. J. Res. Phys. Chem. Chem. Phys. **215**, 401 (2001).
[73] M. Y. Choi and R. E. Miller, J. Am. Chem. Soc. **128**, 7320 (2006).
[74] W. Wewer and F. Stienkemeier, Phys. Rev. B **67**, 125201 (2003).
[75] O. Birer, P. Moreschini, K. K. Lehmann, *et al*., J. Phys. Chem. A **111**, 7624 (2007).
[76] O. Birer, P. Moreschini, K. K. Lehmann, *et al*., J. Phys. Chem. A **111**, 12200 (2007); DOI. 10.1021/jp071175z.
[77] F. Stienkemeier, W. E. Ernst, J. Higgins, *et al*., J. Chem. Phys. **102**, 615 (1995).
[78] F. Stienkemeier, J. Higgins, W. E. Ernst, *et al*., Phys. Rev. Lett. **74**, 3592 (1995).
[79] F. Stienkemeier, J. Higgins, W. E. Ernst, *et al*., Z. Phys. B **98**, 413 (1995).
[80] F. Stienkemeier, J. Higgins, C. Callegari, *et al*., Z. Phys. D **38**, 253 (1996).
[81] A. Bartelt, J. D. Close, F. Federmann, *et al*., Phys. Rev. Lett. **77**, 3525 (1996).
[82] A. Bartelt, J. D. Close, F. Federmann, *et al*., Z. Phys. D **39**, 1 (1997).
[83] F. Stienkemeier, F. Meier, and H. O. Lutz, J. Chem. Phys. **107**, 10816 (1997).
[84] C. Callegari, J. Higgins, F. Stienkemeier, *et al*., J. Chem. Phys. **102**, 95 (1998).
[85] J. Higgins, C. Callegari, J. Reho, *et al*., J. Chem. Phys. **102**, 4952 (1998).

[86] J. Reho, U. Merker, M. R. Radcliff, *et al*., J. Chem. Phys. **112**, 8409 (2000).
[87] J. Reho, J. Higgins, C. Callegari, *et al*., J. Chem. Phys. **113**, 9686 (2000).
[88] J. Reho, J. Higgins, M. Nooijen, *et al*., J. Chem. Phys. **115**, 10265 (2001).
[89] F. Dalfovo, Z. Phys. D **29**, 61 (1994).
[90] F. Ancilotto, E. Cheng, M. W. Cole, *et al*., Z. Phys. B **98**, 323 (1995).
[91] A. Hernando, R. Mayol, M. Pi, *et al*., J. Phys. Chem. A **111**, 7303 (2007).
[92] J. H. Reho, U. Merker, M. R. Radcliff, *et al*., J. Phys. Chem. A **104**, 3620 (2000).
[93] J. Higgins, W. E. Ernst, C. Callegari, *et al*., Phys. Rev. Lett. **77**, 4532 (1996).
[94] J. Higgins, T. Hollebeek, J. Reho, *et al*., J. Chem. Phys. **112**, 5751 (2000).
[95] P. Soldan, M. T. Cvitas, and J. M. Hutson, Phys. Rev. Lett. **67**, 054702 (2003).
[96] J. J. Hurly and M. R. Moldover, J. Res. Natl. Inst. Stand. Technol. **105**, 667 (2000).
[97] J. J. Hurly, K. A. Gillis, J. B. Mehl, *et al*., Int. J. Thermophys. **24**, 1441 (2003).
[98] J. B. Anderson, C. A. Traynor, and B. M. Boghosian, J. Chem. Phys. **99**, 345 (1993).
[99] K. T. Tang, J. P. Toennies, and C. L. Yiu, Phys. Rev. Lett. **74**, 1546 (1995).
[100] T. van Mourik and J. H. van Lenthe, J. Chem. Phys. **102**, 7479 (1995).
[101] H. L. Williams, T. Korona, R. Bukowski, *et al*., Chem. Phys. Lett. **262**, 431 (1996).
[102] T. Korona, H. L. Williams, R. Bukowski, *et al*., J. Chem. Phys. **106**, 5109 (1997).
[103] T. van Mourik and T. H. Dunning Jr, J. Chem. Phys. **111**, 9246 (1999).
[104] J. van de Bovenkamp and F. B. van Duijneveldt, J. Chem. Phys. **110**, 11141 (1999).
[105] R. J. Gdanitz, Mol. Phys. **96**, 1423 (1999).
[106] J. B. Anderson, J. Chem. Phys. **115**, 4546 (2001).
[107] W. Klopper, J. Chem. Phys. **115**, 761 (2001).
[108] M. Jeziorska, R. Bukowski, W. Cencek, *et al*., Collect. Czech. Chem. Commun. **68**, 463 (2003).
[109] W. Cencek, M. Jeziorska, R. Bukowski, *et al*., J. Phys. Chem. A **108**, 3211 (2004).
[110] J. B. Anderson, J. Chem. Phys. **120**, 9886 (2004).
[111] K. Patkowski, W. Cencek, M. Jeziorska, *et al*., J. Phys. Chem. A **111**, 7611 (2007); DOI. 10.1021/jp071437x.
[112] M. Jeziorska, W. Cencek, K. Patkowski, *et al*., J. Chem. Phys. **127**, 124303 (2007).
[113] K. Szalewicz, K. Patkowski, and B. Jeziorski, in *Structure and Bonding: Intermolecular Forces and Clusters*, edited by D. J. Wales, (Springer-Verlag, Heidelberg, 2005), Vol. 116, pp. 43–117.
[114] B. Jeziorski, R. Moszyński, and K. Szalewicz, Chem. Rev. **94**, 1887 (1994).
[115] K. Szalewicz, R. Bukowski, and B. Jeziorski, in *Theory and Applications of Computational Chemistry: The First 40 Years. A Volume of Technical and Historical Perspectives*, edited by C. E. Dykstra, G. Frenking, K. S. Kim, and G. E. Scuseria (Elsevier, Amsterdam, 2005), pp. 919–962.
[116] M. Urban, J. Noga, S. J. Cole, *et al*., J. Chem. Phys. **83**, 4041 (1985).
[117] K. Raghavachari, G. W. Trucks, J. A. Pople, *et al*., Chem. Phys. Lett. **157**, 479 (1989).
[118] H. J. Monkhorst, B. Jeziorski, and F. E. Harris, Phys. Rev. A **23**, 1639 (1981).
[119] C. Møller and M. S. Plesset, Phys. Rev. **46**, 618 (1934).
[120] S. F. Boys and F. Bernardi, Mol. Phys. **19**, 553 (1970).
[121] F. B. van Duijneveldt, J. G. C. M. van Duijneveldt-van de Rijdt, and J. H. van Lenthe, Chem. Rev. **94**, 1873 (1994).
[122] R. Bukowski, B. Jeziorski, and K. Szalewicz, J. Chem. Phys. **104**, 3306 (1996).
[123] T. Korona, and R. Moszyński, and B. Jeziorski, Adv. Quantum Chem. **28**, 171 (1997).
[124] K. Szalewicz and B. Jeziorski, J. Chem. Phys. **109**, 1198 (1998).
[125] K. Patkowski, K. Szalewicz, and B. Jeziorski, J. Chem. Phys. **125**, 154107 (2006).
[126] G. Chałasiński, B. Jeziorski, and K. Szalewicz, Int. J. Quantum Chem. **11**, 247 (1977).
[127] B. Jeziorski, G. Chałasiński, and K. Szalewicz, Int. J. Quantum Chem. **14**, 271 (1978).
[128] B. Jeziorski, W. A. Schwalm, and K. Szalewicz, J. Chem. Phys. **73**, 6215 (1980).
[129] T. Ćwiok, B. Jeziorski, W. Kołos, *et al*., J. Chem. Phys. **97**, 7555 (1992).
[130] K. Patkowski, B. Jeziorski, and K. Szalewicz, J. Chem. Phys. **120**, 6849 (2004).

[131] G. Chalasinski, B. Jeziorski, J. Andzelm, *et al.*, Mol. Phys. **33**, 971 (1977).
[132] K. Szalewicz and B. Jeziorski, Mol. Phys. **38**, 191 (1979).
[133] S. Rybak, K. Szalewicz, and B. Jeziorski, J. Chem. Phys. **91**, 4779 (1989).
[134] S. Rybak, K. Szalewicz, B. Jeziorski, *et al.*, J. Chem. Phys. **86**, 5652 (1987).
[135] P. Jankowski, B. Jeziorski, S. Rybak, *et al.*, J. Chem. Phys. **92**, 7441 (1990).
[136] B. Jeziorski, R. Bukowski, and K. Szalewicz, Int. J. Quantum Chem. **61**, 769 (1997).
[137] R. N. Hill, Int. J. Quantum Chem. **68**, 357 (1998).
[138] B. Jeziorski and K. Szalewicz, Phys. Rev. A **19**, 2360 (1979).
[139] W. Kolos, H. J. Monkhorst, and K. Szalewicz, J. Chem. Phys. **77**, 1323 (1982).
[140] K. Szalewicz, B. Jeziorski, H. J. Monkhorst, *et al.*, Chem. Phys. Lett. **91**, 169 (1982).
[141] B. Jeziorski, H. J. Monkhorst, K. Szalewicz, *et al.*, J. Chem. Phys. **81**, 368 (1984).
[142] K. B. Wenzel, J. G. Zabolitzky, K. Szalewicz, *et al.*, J. Chem. Phys. **85**, 3964 (1986).
[143] S. A. Alexander, H. J. Monkhorst, and K. Szalewicz, J. Chem. Phys. **85**, 5821 (1986).
[144] S. A. Alexander, H. J. Monkhorst, R. D. Roeland, *et al.*, J. Chem. Phys. **93**, 4230 (1990).
[145] R. Bukowski, B. Jeziorski, and K. Szalewicz, J. Chem. Phys. **110**, 4165 (1999).
[146] W. Cencek and K. Szalewicz, Int. J. Quantum Chem. Accepted.
[147] J. Komasa, W. Cencek, and J. Rychlewski, Chem. Phys. Lett. **304**, 293 (1999).
[148] W. Cencek, J. Komasa, K. Pachucki, *et al.*, Phys. Rev. Lett. **95**, 233004 (2005).
[149] K. Pachucki and J. Komasa, J. Chem. Phys. **124**, 064308 (2006).
[150] J. Komasa, W. Cencek, B. Jeziorski, *et al.*, to be published.
[151] F. Luo, C. F. Giese, and W. R. Gentry, J. Chem. Phys. **104**, 1151 (1996).
[152] W. Schollkopf and J. P. Toennies, J. Chem. Phys. **104**, 1155 (1996).
[153] R. E. Grisenti, W. Schollkopf, J. P. Toennies, *et al.*, Phys. Rev. Lett. **85**, 2284 (2000).
[154] A. R. Janzen and R. A. Aziz, J. Chem. Phys. **107**, 914 (1997).
[155] R. A. Aziz, V. P. S. Nain, J. S. Carley, *et al.*, J. Chem. Phys. **70**, 4330 (1979).
[156] R. A. Aziz, F. R. W. McCourt, and C. C. K. Wong, Mol. Phys. **61**, 1487 (1987).
[157] R. A. Aziz and M. J. Slaman, J. Chem. Phys. **94**, 8047 (1991).
[158] B. Liu and A. D. McLean, J. Chem. Phys. **91**, 2348 (1989).
[159] R. J. Vos, J. H. van Lenthe, and F. B. van Duijneveldt, J. Chem. Phys. **93**, 643 (1990).
[160] R. J. Vos, T. van Mourik, J. H. van Lenthe, *et al.*, unpublished results.
[161] V. F. Lotrich and K. Szalewicz, J. Chem. Phys. **112**, 112 (2000).
[162] C. A. Parish and C. E. Dykstra, J. Chem. Phys. **98**, 437 (1993).
[163] C. A. Parish and C. E. Dykstra, J. Chem. Phys. **101**, 7618 (1994).
[164] M. J. Cohen and J. N. Murrell, Chem. Phys. Lett. **260**, 371 (1996).
[165] S.-Y. Hang and M. Boninsegni, J. Chem. Phys. **115**, 2629 (2001).
[166] W. Cencek, M. Jeziorska, O. Akin-Ojo, *et al.*, J. Phys. Chem. A **111**, 11311 (2007); DOI. 10.1021/jp072106n.
[167] V. F. Lotrich and K. Szalewicz, J. Chem. Phys. **106**, 9668 (1997).
[168] V. F. Lotrich and K. Szalewicz, J. Chem. Phys. **106**, 9688 (1997).
[169] V. F. Lotrich and K. Szalewicz, Phys. Rev. Lett. **79**, 1301 (1997).
[170] D. M. Ceperley, Rev. Mod. Phys. **67**, 279 (1995).
[171] S. Stringari and J. Treiner, Phys. Rev. B **36**, 8369 (1987).
[172] T. Biben and D. Frankel, J. Phys.: Cond. Matt. **14**, 9077 (2002).
[173] J. B. Anderson, J. Chem. Phys. **63**, 1499 (1975).
[174] D. Blume, M. Lewerenz, P. Niyaz, *et al.*, Phys. Rev. E **55**, 3664 (1997).
[175] S. Baroni and S. Moroni, Phys. Rev. Lett. **82**, 4745 (1999).
[176] D. M. Ceperley and E. L. Pollock, Phys. Rev. Lett. **56**, 351 (1986).
[177] S. Moroni and M. Boninsegni, J. Low Temp. Phys. **136**, 129 (2004).
[178] H. R. Glyde, R. T. Azuah, and W. G. Stirling, Phys. Rev. B **62**, 14337 (2000).
[179] M. Boninsegni, N. V. Prokofev, and B. V. Svistunov, Phys. Rev. E **74**, 036701 (2006).
[180] S. Grebenev, M. Hartmann, M. Havenith, *et al.*, J. Chem. Phys. **112**, 4485 (2000).

[181] K. Nauta and R. E. Miller, J. Chem. Phys. **113**, 9466 (2000).
[182] K. E. Kuyanov, M. N. Slipchenko, and A. F. Vilesov, Chem. Phys. Lett. **427**, 5 (2006).
[183] M. Behrens, U. Buck, R. Frochtenicht, *et al*., J. Chem. Phys. **109**, 5914 (1998).
[184] M. N. Slipchenko and A. F. Vilesov, Chem. Phys. Lett. **412**, 176 (2005).
[185] K. Nauta and R. E. Miller, Chem. Phys. Lett. **350**, 225 (2001).
[186] R. Moszynski, P. E. S. Wormer, B. Jeziorski, *et al*., J. Chem. Phys. **101**, 2811 (1994).
[187] K. Patkowski, T. Korona, R. Moszyński, *et al*., J. Mol. Struct. (Theochem) **591**, 231 (2002).
[188] M. P. Hodges and R. J. Wheatley, J. Chem. Phys. **114**, 8836 (2001).
[189] G. Calderoni, F. Cargnoni, R. Martinazzo, *et al*., J. Chem. Phys. **121**, 8261 (2004).
[190] D. Blume, M. Lewerenz, F. Huisken, *et al*., J. Chem. Phys. **55**, 8666 (1996).
[191] A. Viel, K. B. Whaley, and R. J. Wheatley, J. Chem. Phys. **127**, 194303 (2007).
[192] B. T. Chang, O. Akin-Ojo, R. Bukowski, *et al*., J. Chem. Phys. **119**, 11654 (2003).
[193] J. Tang and A. R. W. McKellar, J. Chem. Phys. **117**, 2586 (2002).
[194] Y. Z. Zhou and D. Q. Xie, J. Chem. Phys. **120**, 8575 (2004).
[195] X. G. Song, Y. J. Xu, P. N. Roy, *et al*., J. Chem. Phys. **121**, 12308 (2004).
[196] Y. Z. Zhou, D. Q. Xie, and D. H. Zhang, J. Chem. Phys. **124**, 144317 (2006).
[197] G. S. Yan, M. H. Yang, and D. Q. Xie, J. Chem. Phys. **109**, 10284 (1998).
[198] F. Negri, F. Ancilotto, G. Mistura, *et al*., J. Chem. Phys. **111**, 6439 (1999).
[199] T. Korona, R. Moszynski, F. Thibault, *et al*., J. Chem. Phys. **115**, 3074 (2001).
[200] Y. J. Xu, W. Jäger, J. Tang, *et al*., Phys. Rev. Lett. **91**, 163401 (2003).
[201] J. Tang and A. R. W. McKellar, J. Chem. Phys. **121**, 181 (2004).
[202] J. Tang, A. R. W. McKellar, E. Mezzacapo, *et al*., Phys. Rev. Lett. **92**, 145503 (2004).
[203] O. Akin-Ojo, R. Bukowski, and K. Szalewicz, J. Chem. Phys. **119**, 8379 (2003).
[204] R. N. Barnett and K. B. Whaley, J. Chem. Phys. **99**, 9730 (1993).
[205] Y. K. Kwon, D. M. Ceperley, and K. B. Whaley, J. Chem. Phys. **104**, 2341 (1996).
[206] A. Viel and K. B. Whaley, Int. J. Mod. Phys. B, **17**, 5267 (2003).
[207] F. Paesani and K. B. Whaley, J. Chem. Phys. **121**, 5293 (2004).
[208] S. Moroni, A. Sarsa, S. Fantoni, *et al*., Phys. Rev. Lett. **90**, 143401 (2003).
[209] Y. J. Xu, N. Blinov, W. Jäger, *et al*., J. Chem. Phys. **124**, 081101 (2006).
[210] S. Moroni, N. Blinov, and P. N. Roy, J. Chem. Phys. **121**, 3577 (2004).
[211] M. Jeziorska, P. Jankowski, K. Szalewicz, *et al*., J. Chem. Phys. **113**, 2957 (2000).
[212] J. Jakowski, G. Chalasinski, M. M. Szczesniak, *et al*., Chem. Phys. **239**, 573 (1998).
[213] V. F. Lotrich, P. Jankowski, and K. Szalewicz, J. Chem. Phys. **108**, 4725 (1998).
[214] W. Topic, W. Jäger, N. Blinov, *et al*., J. Chem. Phys. **125**, 144310 (2006).
[215] T. Skrbic, S. Moroni, and S. Baroni, J. Phys. Chem. A **111**, 7640 (2007).
[216] J. Tang, Y. J. Xu, A. R. W. McKellar, *et al*., Science **297**, 2030 (2002).
[217] F. Paesani, F. A. Gianturco, and K. B. Whaley, J. Chem. Phys. **115**, 10225 (2001).
[218] Y. Kwon and K. B. Whaley, J. Chem. Phys. **115**, 10146 (2001).
[219] F. Paesani and K. B. Whaley, J. Chem. Phys. **121**, 4180 (2004).
[220] Y. Kwon and K. B. Whaley, J. Phys. Chem. Solids **66**, 1516 (2005).
[221] F. A. Gianturco and F. Paesani, J. Chem. Phys. **113**, 3011 (2000).
[222] K. Higgins and W. Klemperer, J. Phys. Chem. **110**, 1383 (1999).
[223] J. M. M. Howson and J. M. Hutson, J. Chem. Phys. **115**, 5059 (2001).
[224] F. Paesani, A. Viel, F. A. Gianturco, *et al*., Phys. Rev. Lett. **90**, 073401 (2003).
[225] S. Paolini, S. Fantoni, S. Moroni, *et al*., J. Chem. Phys. **123**, 114306 (2005).
[226] R. E. Zillich, F. Paesani, Y. Kwon, *et al*., J. Chem. Phys. **123**, 114301 (2005).
[227] I. Reinhard, C. Callegari, A. Conjusteau, *et al*., Phys. Rev. Lett. **82**, 5036 (1999).
[228] G. Murdachaew, K. Szalewicz, H. Jiang, *et al*., J. Chem. Phys. **121**, 11839 (2004).
[229] K. Harada, K. Tanaka, T. Tanaka, *et al*., J. Chem. Phys. **117**, 7041 (2002).
[230] W. Topic and W. Jäger, J. Chem. Phys. **123**, 064303 (2005).
[231] K. Patkowski, R. Podeszwa, and K. Szalewicz, J. Phys. Chem. A **111**, 12822 (2007).

[232] J. Tang and A. R. W. McKellar, J. Chem. Phys. **119**, 754 (2003).
[233] A. R. W. McKellar, J. Chem. Phys. **121**, 6868 (2004).
[234] A. R. W. McKellar, J. Chem. Phys. **125**, 164328 (2006).
[235] K. von Haeften, S. Rudolph, I. Simanovski, *et al*., Phys. Rev. B **73**, 054502 (2006).
[236] P. Cazzato, S. Paolini, S. Moroni, *et al*., J. Chem. Phys. **120**, 9071 (2004).
[237] S. Moroni and S. Baroni, Comp. Phys. Comm. **169**, 404 (2005).
[238] F. A. Gianturco, M. Lewerenz, F. Paesani, *et al*., J. Chem. Phys. **112**, 2239 (2000).
[239] F. Paesani and F. A. Gianturco, J. Chem. Phys. **116**, 10170 (2002).
[240] T. G. A. Heijmen, T. Korona, R. Moszynski, *et al*., J. Chem. Phys. **107**, 9921 (1997).
[241] C. E. Chuaqui, R. J. Le Roy, and A. R. W. McKellar, J. Chem. Phys. **101**, 39 (1994).
[242] K. A. Peterson and G. C. McBane, J. Chem. Phys. **123**, 084314 (2005); Errata: **124**, 229901 (2006).
[243] A. Conjusteau, C. Callegari, I. Reinhard, *et al*., J. Chem. Phys. **113**, 4840 (2000).
[244] A. A. Mikosz, J. A. Ramilowski, and D. Farrelly, J. Chem. Phys. **125**, 014312 (2006).
[245] B. K. Taylor and R. J. Hinde, J. Chem. Phys. **111**, 973 (1999).
[246] Y. Kwon, F. Paesani, and K. B. Whaley, Phys. Rev. B **74**, 174522 (2006).
[247] A. J. Misquitta and K. Szalewicz, Chem. Phys. Lett. **357**, 301 (2002).
[248] A. J. Misquitta, B. Jeziorski, and K. Szalewicz, Phys. Rev. Lett. **91**, 033201 (2003).
[249] A. J. Misquitta, R. Podeszwa, B. Jeziorski, *et al*., J. Chem. Phys. **123**, 214103 (2005).
[250] R. Podeszwa, R. Bukowski, and K. Szalewicz, J. Chem. Theory Comput. **2**, 400 (2006).
[251] R. Podeszwa, R. Bukowski, B. M. Rice, *et al*., Phys. Chem. Chem. Phys. **9**, 5561 (2007).
[252] A. Viel and K. B. Whaley, in *Advances in Quantum Many-Body Theory*, edited by R.F. Bishop, C. E. Campbell, J. W. Clark, and S. Fantoni (World Scientific, Singapore, 2002), p. 293.
[253] D. T. Moore and R. E. Miller, J. Chem. Phys. **119**, 4713 (2003).
[254] A. Sarsa, Z. Bacic, J. W. Moskowitz, *et al*., Phys. Rev. Lett. **88**, 123401 (2002).
[255] H. Jiang, A. Sarsa, G. Murdachaew, *et al*., J. Chem. Phys. **123**, 224313 (2005).
[256] K. Nauta and R. E. Miller, J. Chem. Phys. **113**, 10158 (2000).
[257] D. R. Willey, V.-E. Choong, and F. C. De Lucia, J. Chem. Phys. **96**, 898 (1992).
[258] Y. Zhang and H.-Y. Shi, J. Mol. Struct. (Theochem) **589**, 89 (2002).
[259] C. M. Lovejoy and D. J. Nesbitt, J. Chem. Phys. **93**, 5387 (1990).
[260] M. J. Elrod and R. J. Saykally, J. Chem. Phys. **103**, 933 (1995).
[261] M. D. Schuder, C. M. Lovejoy, D. D. Nelson, *et al*., J. Chem. Phys. **91**, 4418 (1989).
[262] M. Ortlieb, O. Birer, M. Letzner, *et al*., J. Phys. Chem. A **111**, 12192 (2007).
[263] D. Skvortsov, R. Sliter, M. Y. Choi, *et al*., J. Chem. Phys. (2008), submitted.
[264] R. E. Zillich, Y. Kwong, and K. B. Whaley, Phys. Rev. Lett. **93**, 250401 (2004).
[265] H. Hoshina, J. Lucrezi, M. N. Slipchenko, *et al*., Phys. Rev. Lett. **94**, 195301 (2005).
[266] Y. Kwon and K. B. Whaley, J. Chem. Phys. **119**, 1986 (2003).
[267] K. J. Higgins, Z. Yu, and W. Klemperer, unpublished (2002).
[268] L. C. van den Bergh and J. A. Schouten, J. Chem. Phys. **89**, 2336 (1988).
[269] S. Grebenev, B. Sartakov, J. P. Toennies, *et al*., J. Chem. Phys. **114**, 617 (2001).
[270] F. Paesani and K. B. Whaley, J. Chem. Phys. **124**, 234310 (2006).
[271] U. Buck, F. Huisken, A. Kohlhase, *et al*., J. Chem. Phys. **78**, 4439 (1983).
[272] P. Jankowski and K. Szalewicz, J. Chem. Phys. **108**, 3554 (1998).
[273] P. Jankowski and K. Szalewicz, J. Chem. Phys. **123**, 104301 (2005).
[274] S. Moroni, M. Botti, S. De Palo, *et al*., J. Chem. Phys. **122**, 094314 (2005).
[275] D. T. Moore and R. E. Miller, J. Chem. Phys. **118**, 9629 (2003).
[276] D. T. Moore and R. E. Miller, J. Phys. Chem. A **107**, 10805 (2003).
[277] D. T. Moore and R. E. Miller, J. Phys. Chem. A **108**, 1930 (2003).
[278] H. Jiang and Z. Bacic, J. Chem. Phys. **122**, 244306 (2005).
[279] F. Sebastianelli, Y. S. Elmatad, H. Jiang, *et al*., J. Chem. Phys. **125**, 164313 (2006).
[280] F. Paesani, K. B. Whaley, G. E. Douberly, *et al*., J. Phys. Chem. A **111**, 7516 (2007).

[281] G. E. Douberly, J. M. Merritt, and R. E. Miller, J. Phys. Chem. A **111**, 7282 (2007).
[282] F. Paesani, (2007), private communication.
[283] E. W. Draeger, K. K. Lehmann, G. E. Douberly, *et al.*, The microscopic Andronikashvili experiment as a probe of superfluid helium excitations (2003), unpublished.
[284] J. M. Hutson, J. Chem. Phys. **96**, 6752 (1992).
[285] V. F. Lotrich, H. L. Williams, K. Szalewicz, *et al.*, J. Chem. Phys. **103**, 6076 (1995).
[286] A. R. Cooper, S. Jain, and J. M. Hutson, J. Chem. Phys. **98**, 2160 (1993).
[287] A. Ernesti and J. M. Hutson, Phys. Rev. A **51**, 239 (1995).
[288] A. Ernesti and J. M. Hutson, J. Chem. Phys. **106**, 6288 (1997).
[289] C. J. Burnham, S. S. Xantheas, M. A. Miller, *et al.*, J. Chem. Phys. **117**, 1109 (2002).
[290] R. Bukowski, K. Szalewicz, G. C. Groenenboom, *et al.*, Science **315**, 1249 (2007).
[291] G. E. Douberly and R. E. Miller, J. Phys. Chem. B **107**, 4500 (2003).
[292] M. Douglas and N. M. Kroll, Ann. Phys. **82**, 89 (1974).
[293] R. J. Hinde, J. Phys. B: At. Mol. Opt. Phys. **36**, 3119 (2003).
[294] G. C. Groenenboom, E. M. Mas, R. Bukowski, *et al.*, Phys. Rev. Lett. **84**, 4072 (2000).
[295] G. C. Groenenboom, P. E. S. Wormer, A. van der Avoird, *et al.*, J. Chem. Phys. **113**, 6702 (2000).
[296] R. A. Aziz, A. R. Janzen, and M. R. Moldover, Phys. Rev. Lett. **74**, 1586 (1995).